SPIN COATED FILMS OF INORGANIC COMPLEXES AND A STUDY OF THE PHOTOCHEMISTRY OF METAL COMPLEXES WITH HALOGEN LIGANDS

by Christina Iren Horvath

B.Sc., Simon Fraser University, 1992

THESIS SUBMITTED IN PARTIAL FULFILLMENT OF THE REQUIREMENTS

FOR THE DEGREE OF MASTER OF SCIENCE

in the Department

of

Chemistry

Simon Fraser University

May 1997

Approval

Name: Christina Iren Horvath

Degree: Master of Science

Title of Thesis: Spin Coated Films of Inorganic Complexes and A Study of the Photochemistry of Metal Complexes with Halogen Ligands

Examining Committee

Chairperson: Dr. D. Sutton

Dr. R.H. Hill, Senior Supervisor

Dr. F.W.B. Einstein

Dr. S. Holdcroft

Dr. J. D'Auria, Internal Examiner
Chemistry, SFU

Date Approved May 8, 1997

Abstract

Spin coated thin films of metal complexes serve as useful precursors in the photodeposition of metal and metal oxide films. The ability to control the film thickness and morphology is essential to industrial applications of metal based films. Furthermore, potential industrial applications require that the photodeposition process be efficient and cost effective.

A comparison was made of different spin coating conditions for $Ni(PEt_3)_2X_2$ and $Ni(PPh_3)_2X_2$. It was found that controlling the outcome of spin coating a film involves a complex combination of variables. Low spin speeds (<500 rev/min) produced thicker films. However, the resulting films were in a crystalline phase; and amorphous films are preferred for photochemistry. Fortunately, the degree of crystallinity in the film was also affected by the ligands on the metal centre. For example, films of the relatively large tetrahedral $Ni(PPh_3)_2I_2$ did not crystallize as readily as the films of the relatively small square planar $Ni(PEt_3)_2Cl_2$. Thicker films were also produced when the complexes were spin coated from high concentration precursor solutions made with solvents of low boiling point. Comparisons of the results of the conditions of spin coating were made with studies of spin coated polymers. Qualitatively, the results matched in spin speed and precursor solution concentration. The mathematical relationships of spin speed and precursor solution concentration did not always parallel the mathematical relationships for polymer films.

Spin coated films of $CpFe(CO)_2X$, $Ni(PEt_3)_2X_2$ and $Ni(PPh_3)_2X_2$ (X=Cl, Br, I) were photolyzed. The main objective of the study was to determine if halogen ligands are

ejected upon photolysis. Analysis by energy dispersive spectroscopy and Auger electron spectroscopy of a photolyzed film of $CpFe(CO)_2I$ indicated that the film had reacted to form an oxide of iron. The halogen ligands were not likewise ejected from the films of $CpFe(CO)_2Cl$ and $CpFe(CO)_2Br$. This was attributed to the stronger Fe-Cl and Fe-Br bonds compared to the bond strength of Fe-I. None of the films of nickel complexes formed metal or metal oxide films. The photochemistries of these complexes were complicated by simultaneous thermal reactions. The thermal and photochemical reaction of $Ni(PEt_3)_2I_2$ were not clearly distinguished and therefore conclusions were not made on this compound. Analysis of the photoproducts of the films of $Ni(PEt_3)_2Cl_2$ and $Ni(PEt_3)_2Br_2$ showed the films were consistent with films of $NiCl_2$ and $NiBr_2$. The infrared spectra of the final films showed loss of the phosphine ligands and the Auger spectra indicated that the halogens had not escaped the films. The photochemistries of the films of $Ni(PPh_3)_2X_2$ resulted in the formation of the $Ni(OPPh_3)_2X_2$ for all three analogues. Upon photolysis of the films of $Ni(PPh_3)_2X_2$, infrared bands appeared that are consistent with $OPPh_3$. The success of producing an oxide of iron by photolysis of a film of $CpFe(CO)_2I$ demonstrates that metal complexes with halogen ligands are viable precursors in the photodeposition of metal and metal oxide films.

Dedication

To my parents, George and Helen Horvath,
with lots of love

Acknowledgments

I wish to thank my supervisor Dr. Ross H. Hill for his support and guidance.

I wish to thank my husband Dr. Jose R. Marino Albernas for all of his love, and support. I could not have done it without you Jose.

A thank you also goes to Dr. Sharon Blair and the Physics Department for the Auger analyses. And a thank you goes to Dr. Curzon's laboratory group in the Physics Department for the EDS analysis.

I wish to thank my groupmates for their help and friendship.

Finally I wish to acknowledge the generous financial support from Dr. Ross H. Hill, NSERC, the Chemistry Department and Simon Fraser University.

Table of Contents

List of Tables

List of Figures

List of Abbreviations

AES: Auger electron spectroscopy

Cp: cyclopentadienyl

CVD: chemical vapour deposition

EDS: Energy dispersive spectroscopy

PVD: physical vapour deposition

X: a halogen ligand

Chapter 1. Introduction

This thesis presents an investigation of the variables that affect the thickness and morphology of thin films spin coated from metal complexes in solution. Studies on nickel complexes of the type $Ni(PR_3)_2X_2$ (R=Et, and Ph; X=Cl, Br, and I) were investigated to help researchers optimize conditions for the spin coating of other metal complexes. This thesis also presents the photochemistry of a series of films made from complexes that have halogen ligands. Their potential as precursor films in the photoproduction of metal and metal oxide films is assessed. The complexes for the films in the photochemistry study include $Ni(PR_3)_2X_2$ and $CpFe(CO)_2X$ (X=Cl, Br, and I).

Chapter one serves as an introduction to many of the topics discussed in the thesis. Some techniques of thin film production and film patterning are described in sections 1.1 and 1.2 respectively. Section 1.3 discusses the importance of some of the characteristics of solid films. The next two sections of this chapter describe the research goals and plans of the thesis. Finally in section 1.6, there is a description of the surface analysis techniques that were used.

1.1 The relevance of studying thin films.

There are many applications of thin solid films. Simple examples include decorative arts and protective coatings against heat, mechanical wear or chemical erosion. Memory discs, liquid/gas sensors and antireflective coatings are a few more of the many applications of thin films.[1] One of the most lucrative applications of thin solid films is in

the microelectronics industry. Different types of thin films are used in this industry. For example, films of metals, metal oxides and polymers may all be used in integrated circuits. These films can be made by a variety of techniques; and these films are often deposited in patterned formations.

1.2. Techniques of making thin films.

The techniques for making thin films with applications in microelectronics are physical vapour deposition, chemical vapour deposition, and spin coating.[10] This set of methods can be used for the production of metal, metal oxide, metal complex or organic polymeric films. There are also different ways of patterning the films that are made. A description of methods of film production and patterning is in the following text.

a. Physical Vapour Deposition (PVD):[2-5] Metal oxide, metal and alloy films can be made by this method.[4] A sample of metal is put into the vapour phase for transport to a selected substrate. The energy source to vapourize the solid may be heat, or a beam of electrons, photons (laser ablation), or positive ions (sputtering).[2-5] The vapour then condenses on the substrate. The transport of atoms or molecules can occur in vacuum or in high pressures.[5]

b. Chemical Vapour Deposition (CVD):[2, 3, 5] In CVD, the source materials are in the gas phase. The source material reacts chemically to form a new material which deposits atomistically on the substrate.[1] The transport of the atoms or molecules to the substrate can occur via a vacuum, at high pressures or within a plasma.[2, 5] CVD is activated or

assisted by heat, laser excitation, ultra violet energy, an electron beam, or an ion beam.[2, 5] For example, films of Gallium Arsenide (GaAs) can be made by this technique.[5]

c. Spin Coating:[6] A solution of a metal complex, or a polymer in liquid solvent is dispensed on a spinning substrate as illustrated in Figure 1.1. Much of the solution dispenses off, but some of the solute adheres to the substrate. The substrate is left spinning to allow residual solvent to evaporate. Spin coated films are often further processed thermally or photolytically to obtain the final product. Films of polymers or metal complexes are made by this technique.

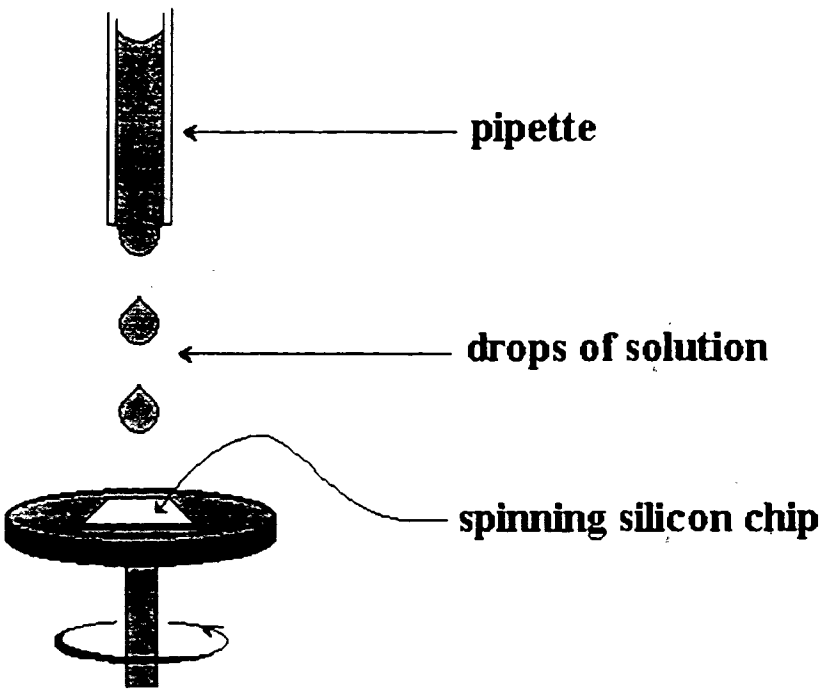

Figure 1.1. Illustration of the spin coating technique.

1.3. Techniques of film patterning.

Different techniques are available to pattern a film. The choice depends on the nature of the thin film, its thickness and the pattern resolution required for the application. Various techniques of patterning will be described.

A film of a metal or metal oxide made by PVD or CVD can be directly etched by a mechanical mask, stencil or a beam writer. In the case of the mechanical mask and stencil, the vapour or gas condenses on the substrate through patterned areas.[5] An alternate method for patterning films made by photoassisted CVD, is beam writing. Light is focused on the photosensitive vapour in the design of the desired pattern. The only molecules that react and condense to form a film are those in the path of the beam.[5] The disadvantage of these methods is that the resolutions achieved are not always sufficient for applications in microelectronics.

Industry currently uses photolithographic masks and photosensitive polymer films called photoresists in order to achieve high resolution patterns of metal and metal oxide films made by PVD or CVD. Films made by PVD and CVD cannot be patterned directly by photolithography because films made by these methods are not photosensitive. Figure 1.2 illustrates the general process of photolithography of a photoresist to pattern a film of a metal or metal oxide.[10]

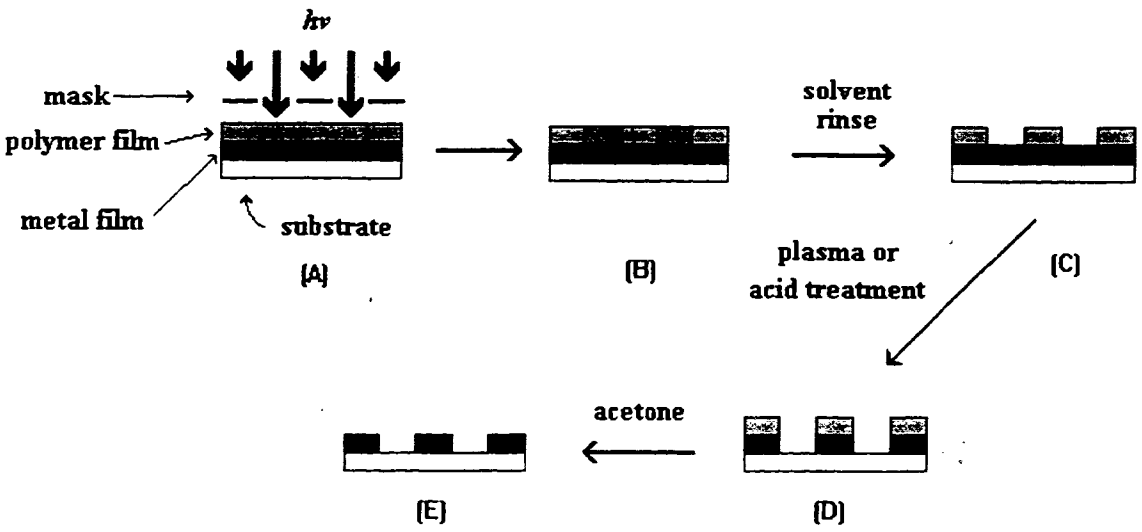

Figure 1.2 Photolithographic processing using a photoresist.

The starting material (figure 1.2.A) is composed of a substrate, a metal or a metal oxide film, and a spin coated polymer film (photoresist). The metal or metal oxide film, which is made by a vapour deposition technique, is sandwiched between the substrate and the photoresist. The polymer film is selectively photolyzed through a photolithographic mask. The reacted areas of polymer (figure 1.2.B) have different solubility properties than the unreacted areas of the polymer film. A solvent rinse selectively washes away the photoreacted areas of polymer (or the unreacted areas depending upon the system). Selected areas of the metal or metal oxide film (figure 1.2.C) are now exposed to the atmosphere, and can be corroded away using a plasma or acid treatment to give a patterned film of metal or metal oxide (figure 1.2.D). The remaining polymer film is then rinsed away with acetone. The final product (figure 1.2.E) is a patterned film made of metal or metal oxide.

The process of patterning a film of metal or metal oxide by using a photoresist is a lengthy multistep process. In contrast, a much shorter method is the photolithography of

an inorganic complex to produce a patterned film of a metal or metal oxide. Figure 1.3 outlines the latter process.

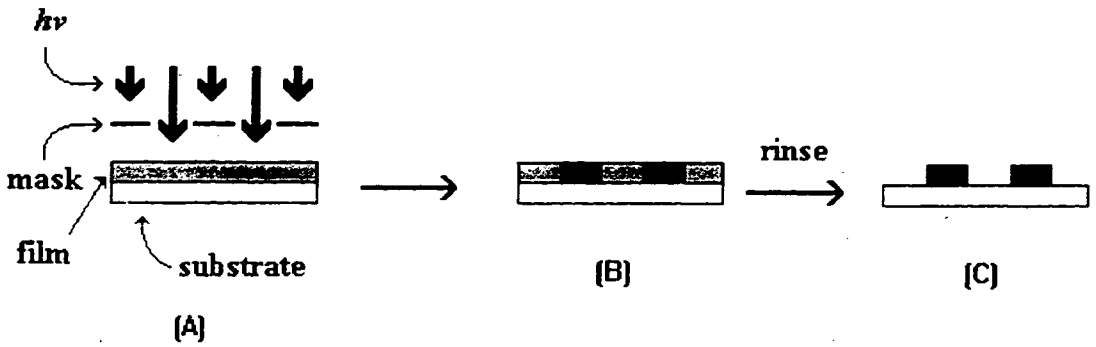

Figure 1.3 Photolithographic processing of an inorganic complex.

A thin film of an inorganic complex, obtained by the spin coating technique on a substrate, is photolyzed through a photolithographic mask (figure 1.3.A). The exposed areas of the film selectively react under the light to form a film of a metal or metal oxide (figure 1.3.B). The unexposed areas remain as an inorganic complex and therefore can be rinsed away with solvent. Figure 1.3.C shows the final product which is a substrate with a pattern of metal or metal oxide on top.

The method of making patterned thin films of metal or metal oxides by photolithography of inorganic complexes is simpler and requires fewer steps than current industrial technology (photolithography using a photoresist, figure 1.2.). Therefore, the industrial application of the photolithographic method of inorganic complexes would be less costly. To apply this method to industrial settings, the process of spin coating the inorganic complex must be better understood. For instance, film thickness and film morphology are two important characteristics of the film which need to be more controllable to make the technology transferable to industry.

1.4. The importance of the film thickness and film quality.

One of the important characteristics of a thin film is its thickness.[3] For example, conductance of electricity through a thin film is dependent on the thickness of the film. If the film is too thin, the resistance of the film is very high. Therefore, in microelectronic devices, the ideal film must be sufficiently thick to be a good conductor of electricity.

The morphology of a film is another important feature. It has been shown that a film of an inorganic complex which is optically amorphous readily photoejects ligands.[11] In contrast films which are optically crystalline do not readily photoeject ligands. A lattice structure is highly ordered and rigid, making it difficult for dissociated ligands to escape the film.

1.5. Goals and strategies of studying spin coating variables.

The goal of this study is to determine the conditions of spin coating metal complexes that affect the film thickness and morphology of a film. The information gained from the investigation can be used as a guide in the development of films of other complexes.

The variables of spin coating were studied by making a series of films of six different metal complexes under various conditions. The complexes were $Ni(PEt_3)_2X_2$ and $Ni(PPh_3)_2X_2$ (X=Cl, Br, I). These complexes provided a set of molecules with trends in size, and geometry[14-21] that can be compared to the trends found in the spin coated films of

these complexes. Film thickness and the morphology were examined after the films were spin coated under different conditions. Infrared spectra of the films were used to determine the thicknesses of the films and a light microscope was used to examine the morphologies. Parameters of spin speed, solution concentration, and solvent properties were examined to find correlations with the resulting film thicknesses and film morphologies.

1.6. Goals and strategies of studying the photochemistry of the films of metal complexes with halogen ligands.

The photochemistry of films of a group of metal complexes with halogen ligands was studied. There are a wide variety of metal complexes with halogen ligands available that could serve as valuable precursor films. Their use depends largely on the efficiency of the photoejection of the halogen ligands from the films to form films of metal or metal oxide as shown in equation 1.1 and 1.2. Films of complexes with other ligands have been shown to photodeposit metal and metal oxide films.[7,24,67] This study will give an indication of the viability of using films of metal complexes with halogen ligands as well.

$$ML_mX_n \xrightarrow{h\nu} M + mL + nX \qquad (1.1)$$

$$nM + mO_2 \longrightarrow M_nO_{2m} \qquad (1.2)$$

The photochemistry of films of $Ni(PEt_3)_2X_2$ and $Ni(PPh_3)_2X_2$ and $CpFe(CO)_2X$ (X=Cl, Br, I) were studied in the evaluation of metal complexes with halogen ligands. All of the films were spin coated onto silicon wafers by the method described in Section 1.1.

Throughout the photolysis of each film, several infrared spectra were taken of the films. The intensities of the infrared bands were monitored until the spectra remained constant with exposure to light. Those photolyzed films which had infrared spectra that were consistent with a metal or metal oxide film were further analyzed by Auger electron spectroscopy (AES), and in one case by energy dispersive spectroscopy (EDS) as well. These surface techniques indicated the ratios of elements of the photoproduct film. Further explanation of AES and EDS is in section 1.7.

1.7. Analysis of thin films by AES and EDS.

Surface analysis of thin films was performed by Auger electron spectroscopy (AES) and energy dispersive spectroscopy (EDS). These methods are complimentary methods which indicate the elemental ratios of surfaces.

In Auger electron spectroscopy (AES) atoms of the surface material undergo non-radiative decay resulting in the ejection of one of the outer electrons. The kinetic energy of the ejected electron (the Auger electron) is characteristic of an element. A schematic diagram of the process is in Figure 1.4.

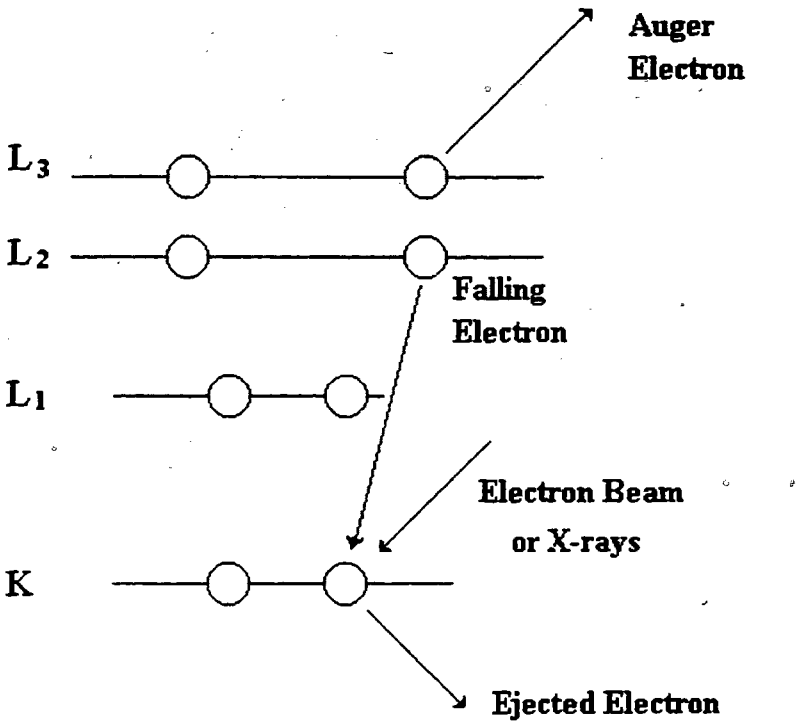

Figure 1.4 Schematic diagram of the Auger process notated by $KL_{2,3}L_{2,3}$.[22, 23]

The first step of the production of Auger electrons is the ionization of the inner shell by electron bombardment or x-rays. An electron then falls in energy from a higher energy level to fill the core hole. The energy release from this process provides kinetic energy for the emission of an Auger electron. Elements are identified by the kinetic energy of their Auger electrons. AES is also described by equation 1.3.[22, 23]

$$E_A=E_1-E_2-E_3-U \qquad (1.3)$$

E_A=kinetic energy of the Auger electron
E_1=binding energy of the electron that is intially ejected
E_2=binding energy of the electron that drops into the created hole
E_3=energy of the detected Auger electron
U=hole-hole repulsion energy

The method of quantifying results of Auger electron spectroscopy uses the sensitivity of elements determined by standards elemental samples. Equation 1.4 is applied to determine the relative quantities of the elements.

$$C_i=(I_i/S_i)/\Sigma(I_i/S_i) \qquad (1.4)$$

C_i is the concentration of the *i*th component
S_i is the *i*th elemental sensitivity factor
I_i is the current of emitted Auger electrons
$\Sigma(I_i/S_i)$ is the summation of (I_i/S_i) ratio of all elements detected in the Auger spectrum

Energy dispersive spectroscopy (EDS) can also be used to analyze the relative amounts of elements of a solid surface.[8] A beam of electrons ejects an electron of the inner shell and another electron falls in energy to fill the vacancy of the inner shell. The energy difference between the shells may be emitted as anx-ray. The energy of the x-ray is used to identify the element.

2. Optimizing the Conditions of Spin Coating Metal Complexes

2.1. Introduction

Variables which affect the thickness and morphology of spin coated thin films cast from metal complex solutions are investigated in this chapter. For the purposes of this study, a series of nickel complexes were spin coated into thin films under different conditions of spin coating. The series of nickel complexes selected for the study are $Ni(PEt_3)_2X_2$ and $Ni(PPh_3)_2X_2$ (X=Cl, Br, I). This set of molecules follow a trend in size, polarizability, and geometry[12-18, 25-31] that may result in a trend in film thickness or film continuity.

The conditions of spin coating that were tested were spin speed, solution concentration, solution viscosity, and solvent type. These are a reasonable set of variables to investigate because these same variables have been found to affect the thickness of spin coated polymer films.[2-18, 25-31] The extent to which each variable has impact on the final films and the mathematical relationship of these variables, are useful to maximize ideal conditions of the spin coating of other metal complexes.

2.2. Results

2.2.1 FTIR Spectroscopy and Film Thickness

Infrared spectra were taken of the $Ni(PEt_3)_2Cl_2$. First a spectrum was obtained of the complex in a pellet of KBr. This was done to identify the infrared bands of $Ni(PEt_3)_2Cl_2$

and distinguish them from any bands due to solvent trapped in the film. The bands were at $\rho(CH_2)$[27]727 cm^{-1} (strong), $\rho(CH_2)$[27]764 cm^{-1} (strong), and ν(P-C)[27]1034 cm^{-1} (strong). A film of $Ni(PEt_3)_2Cl_2$ was made by the technique described in Section 1.2 and 2.5.2. The spectrum of the spin coated film of $Ni(PEt_3)_2Cl_2$ was obtained (see Figure 2.1). Absorbance bands in the spectrum were found at 727 cm^{-1} (strong), 764 cm^{-1} (strong), and 1037 cm^{-1} (strong). The error of the infrared instrument is ± 4 cm^{-1} and therefore, the spectrum of the film of $Ni(PEt_3)_2Cl_2$ matches the spectrum of $Ni(PEt_3)_2Cl_2$ in a KBr pellet.

The same procedure was followed for all of the complexes of $Ni(PEt_3)_2X_2$ and $Ni(PPh_3)_2X_2$ (X=Cl, Br and I). The results are tabulated in Table 2.1 and the spectra of the complexes as films are shown in Figures 2.1-2.6.

Table 2.1. Infrared Bands of the $Ni(PR_3)_2X_2$ a.) in a KBr pellet, b.) as a film.

Complex	$\rho(CH_2)$[27]	$\rho(CH_2)$[27]	ν(P-C)[27]
$Ni(PEt_3)_2Cl_2$	727(s), 727 (s)	764(s), 764 (s)	1034(s), 1037 (s)
$Ni(PEt_3)_2Br_2$	721(s), 721 (s)	762(s), 762 (s)	1034(s), 1034 (s)
$Ni(PEt_3)_2I_2$	718(s), 721 (s)	764(s), 762 (s)	1030(s), 1034 (s)
	vibrations of the phenyl ring[56]	vibration of the phenyl ring[56]	ν(P-C)[56]
$Ni(PPh_3)_2Cl_2$	692(s), 696 (s)	746(s), 743 (s)	1095 (m), 1090 (w)
$Ni(PPh_3)_2Br_2$	692(s), 694(s)	745(s), 747(s)	1096 (m), 1097(m)
$Ni(PPh_3)_2I_2$	692(s), 692 (s)	743(s), 743 (s)	1096 (br, s), 1096 (s)

Figure 2.1. Infrared spectrum of $Ni(PEt_3)_2Cl_2$

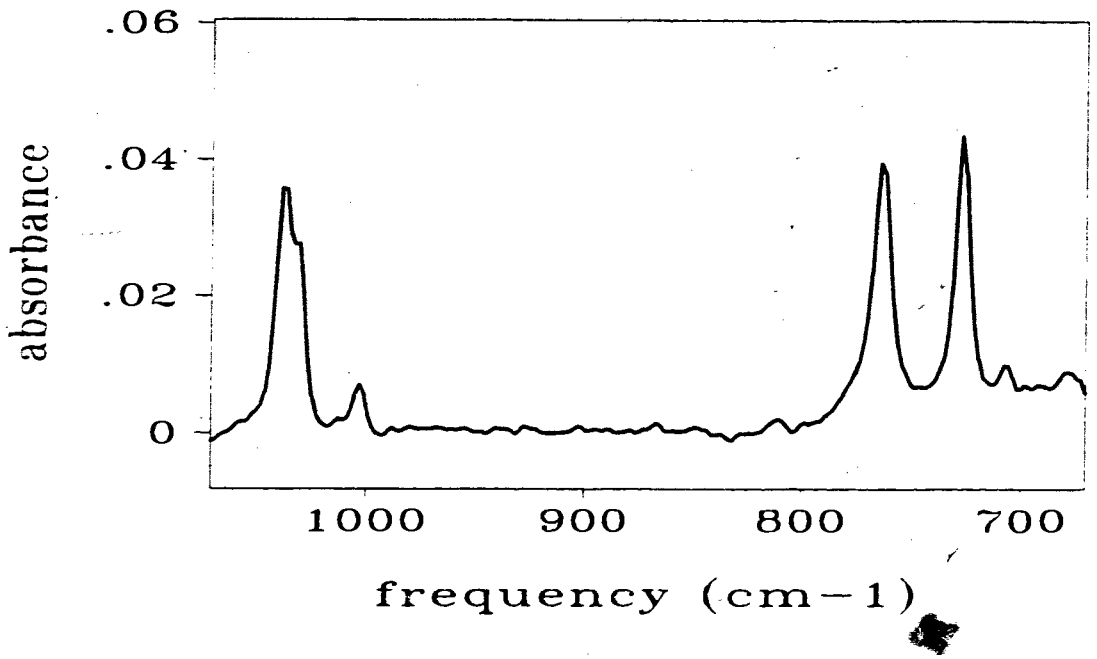

Figure 2.2. Infrared spectrum of $Ni(PEt_3)_2Br_2$

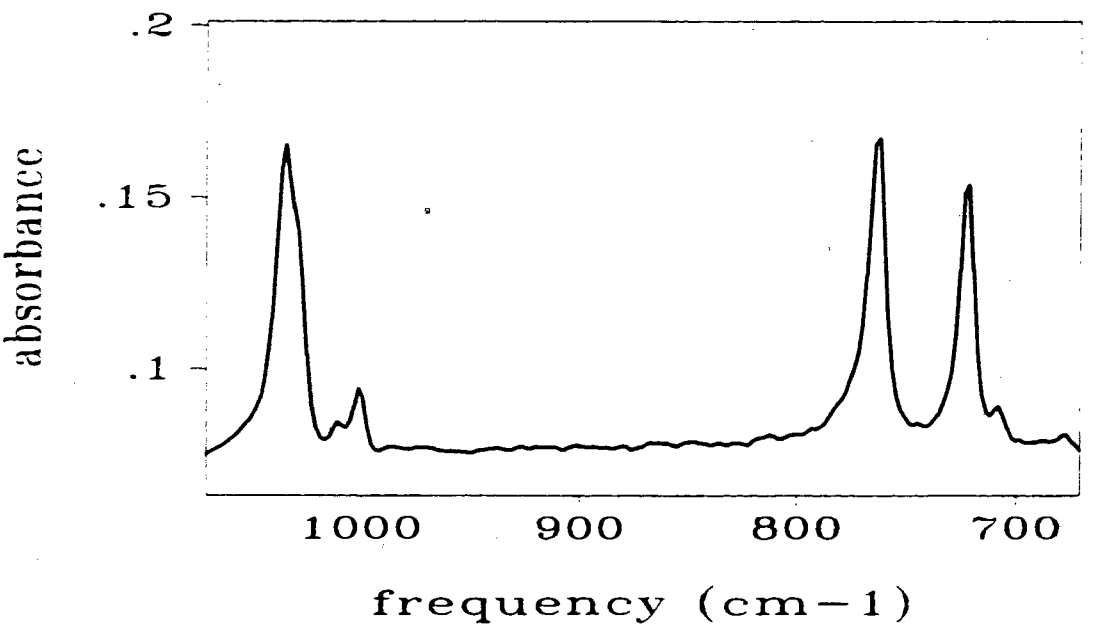

Figure 2.3. Infrared spectrum of $Ni(PEt_3)_2I_2$

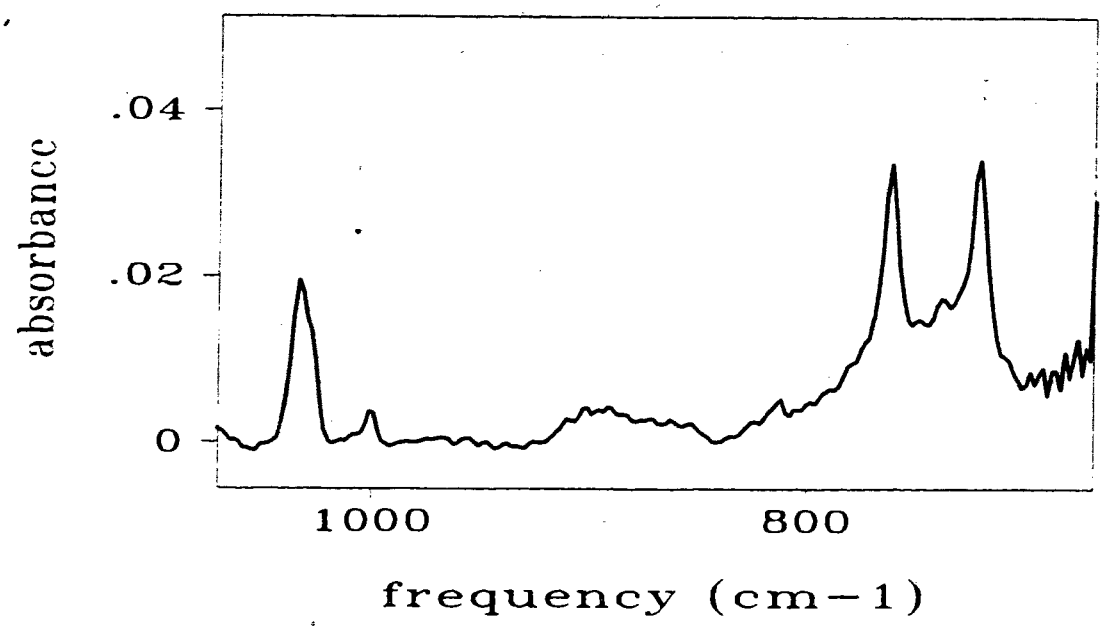

Figure 2.4. Infrared spectrum of $Ni(PPh_3)_2Cl_2$

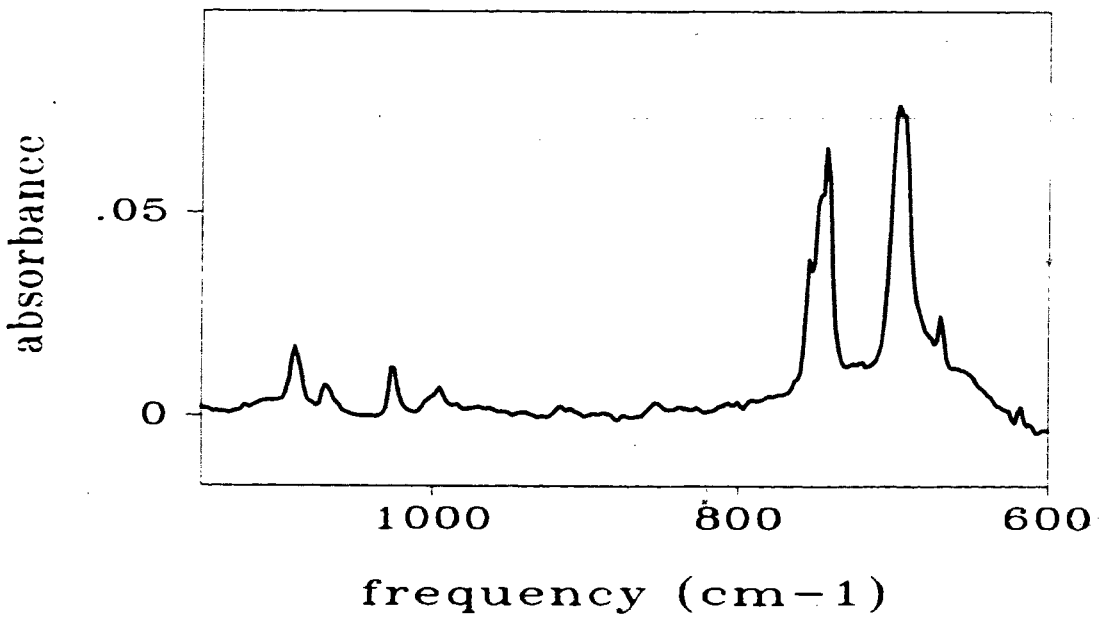

Figure 2.5. Infrared spectrum of $Ni(PPh_3)_2Br_2$

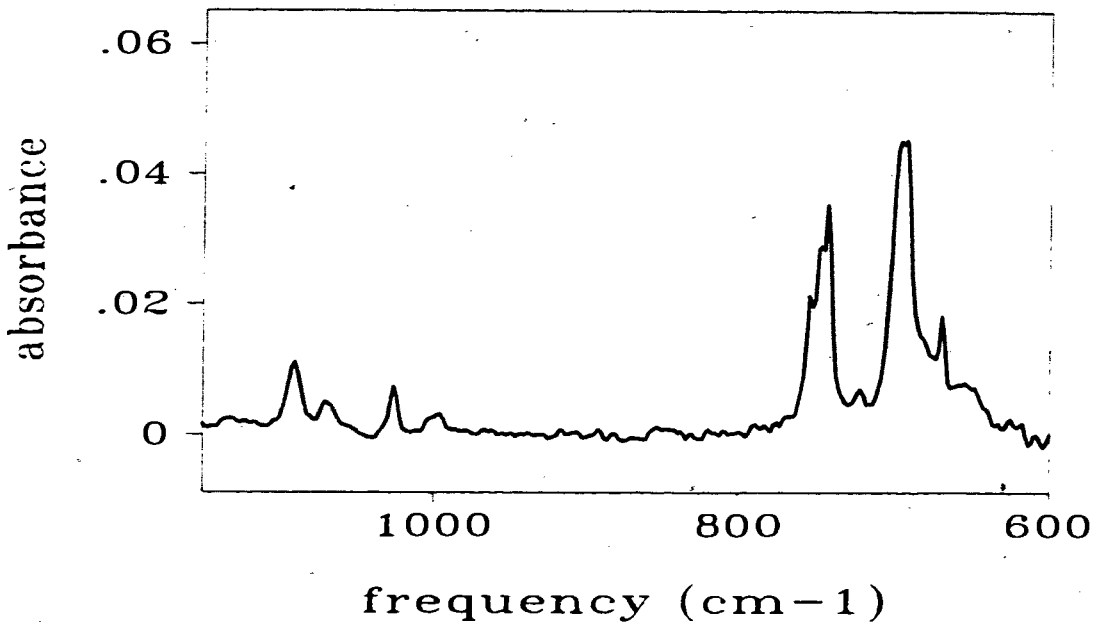

Figure 2.6. Infrared spectrum of $Ni(PPh_3)_2I_2$

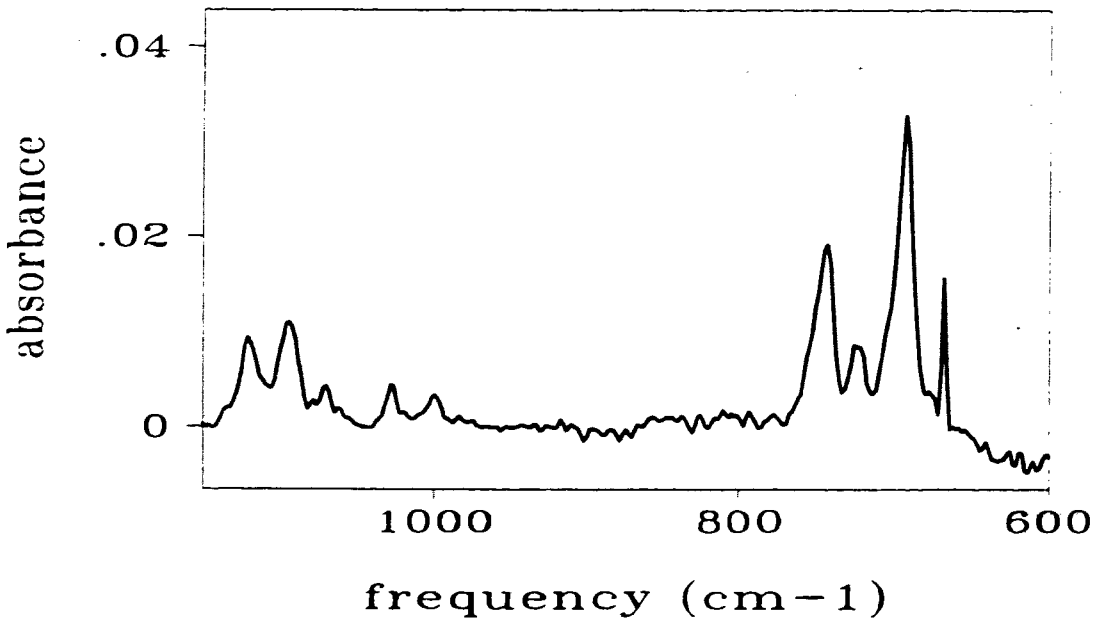

2.2.2. Beer Lambert plots of the complexes.

The average relative thicknesses of films were measured using infrared spectra of the films. Beer-Lambert plots were made to convert the intensity of the absorbance bands of the spectra, in absorbance units, to thickness, in molecules per Ångstrom squared (molecules/Å^2) of the films (section 2.5.4).

The most intense absorbance bands of the complexes were selected for the construction of the calibration plots. In the case of the $Ni(PEt_3)_2Cl_2$ the relative intensities of the absorbance bands at 727 cm^{-1} and 764 cm^{-1} varied slightly with respect to eachother, and therefore the absorbance at 1037 cm^{-1} was used for the calibration plot. Table 2.2 lists the bands that were monitored and the slope of calibration of all of the complexes.

2.2.3. The relationship between concentration of precursor solutions and film thickness of spin coated films.

A series of spin coated films of $Ni(PEt_3)_2Cl_2$ were made from solutions of different concentrations of $Ni(PEt_3)_2Cl_2$ in CH_2Cl_2 ranging from 0.001 to 0.050 M. The spin speed was held constant at 1700 rpm for all of the spin coated films. A graph of absorbance versus solution concentration was fit to a straight line graph using a linear regression fit (Figure 2.7). The slope of this graph was converted from 0.00333 absorbance units/M to 86.5 molecules/Å^2·M using the extinction coefficient obtained from the Beer Lambert plot. The error bars (±0.002 abs. units) of the data were

determined by measuring the maximum differences in baseline intensity between the spectra.

Figure 2.7. Graph of absorbance vs. concentration of $Ni(PEt_3)_2Cl_2$

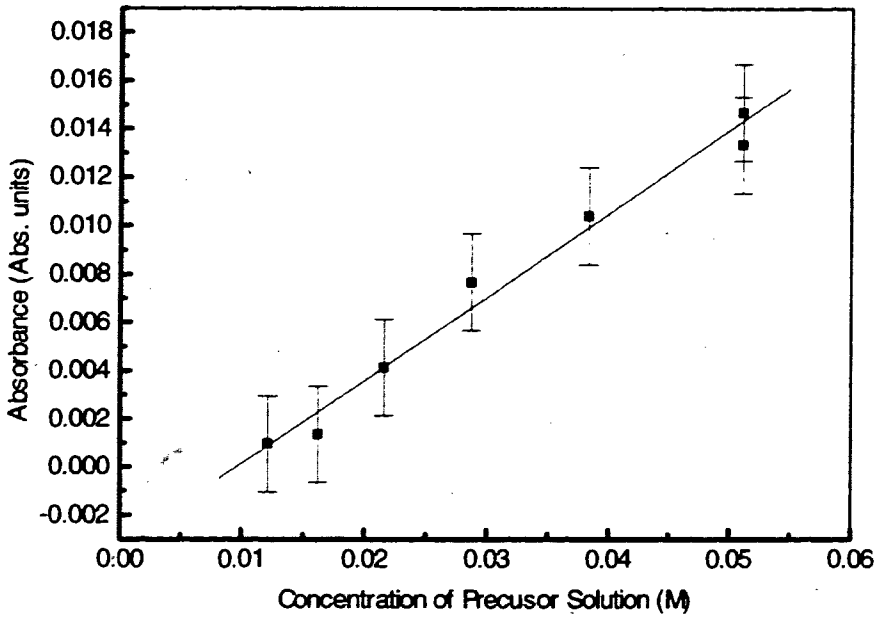

The converted slopes of the six nickel complexes are listed in Table 2.2. The table reveals that the spin coated films of $Ni(PEt_3)_2Cl_2$ and $Ni(PPh_3)_2I_2$ yield the thickest films at a given concentration. The remaining four complexes were substantially thinner and were comparable in thickness to each other.

Table 2.2. Table of extinction coefficients and dependence of film thickness on precursor solution concentration.

Compound	Infrared Band	Extinction Coefficient (Absorbance units /(molecules/Å^2)	Average Thickness (molecules/Å^2*M)
$Ni(PEt_3)_2Cl_2$	1037 cm^{-1}	0.0032±0.0006	110±20
$Ni(PEt_3)_2Br_2$	762 cm^{-1}	0.008±0.002	50±13
$Ni(PEt_3)_2I_2$	760 cm^{-1}	0.0050±14	57±16
$Ni(PPh_3)_2Cl_2$	696 cm^{-1}	0.0080±13	80±30
$Ni(PPh_3)_2Br_2$	692 cm^{-1}	0.0150±.0015	32±5
$Ni(PPh_3)_2I_2$	692 cm^{-1}	0.0058±0.0010	100±20

2.2.4. The relationship between spin speed and film thickness.

A series of spin coated films were made of $Ni(PEt_3)_2Cl_2$ at different spin speeds between 50 and 4000 rpm. The concentration of precursor solution was held constant at 0.018 M. Figure 2.8 shows the relationship between spin speed and film thickness of the film. The thickness was dependent upon spin speed in speeds of 0-500 rpm, but was not measurably dependent upon the spin speed in speeds above 500 rpm. The error bars (±0.002 abs. units) were determined by the difference in intensity of the baselines between the spectra.

Figure 2.8. Graph of Absorbance versus Spin Speed for $Ni(PEt_3)_2Cl_2$.

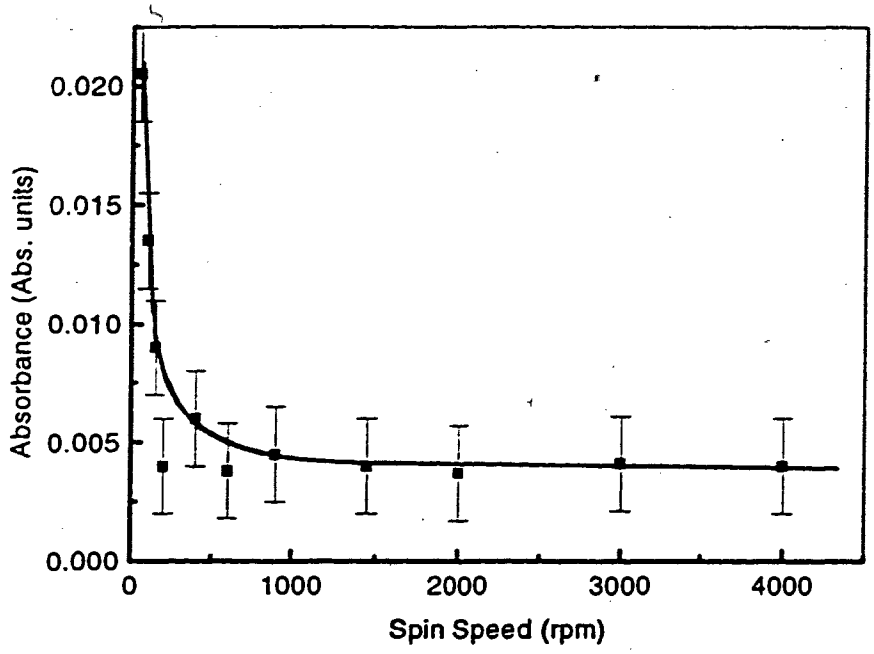

The data points at spin speed = 200 rpm and absorbance = 0.004 abs. units; and spin speed = 600 rpm and absorbance = 0.0038 abs. units are at lower thicknesses than what the overall trend indicates. An explanation for their relative thickness is due to the morphology of the film. Spin coated films of $Ni(PEt_3)_2Cl_2$ appear to contain many crystals at an optical level. Continued spinning of these films may result in some of the crystals sloughing off of the wafer, yielding a film of lesser average thickness. For the purposes of further analyses these two points will not be used.

The same procedure was followed for all of the complexes of $Ni(PEt_3)_2X_2$ and $Ni(PPh_3)_2Cl_2$ (X=Cl, Br, and I). The graphs of absorbance versus spin speed were the same as that for $Ni(PEt_3)_2Cl_2$. Film thickness was dependent upon spin speed when the

film was spin coated at speeds of 50-500 rpm; and there was no measurable dependency on spin speed in speeds of 500-4000 rpm.

2.2.5. The viscosity of the precursor solutions.

The viscosities of the $Ni(PR_3)_2X_2$ /CH_2Cl_2 solutions at approximately the same concentration were measured by a Canon Fenske routine viscometer. The results are listed in Table 2.7 of the experimental section. A significant difference was not found in the viscosities amongst the solutions and therefore the data is not useful in determining if the viscosity of the solution affects the thickness of the spin coated films.

2.2.6. The solubility of the complexes in CH_2Cl_2.

The ultraviolet-visible spectrum of 6.39×10^{-3} M of $Ni(PEt_3)_2Cl_2$ in CH_2Cl_2 was taken. The extinction coefficient was $\varepsilon = 0.926$ mm^{-1} M^{-1} at λ=664 nm. Excess $Ni(PEt_3)_2Cl_2$ was mixed in CH_2Cl_2 and the solution was filtered to obtain a saturated solution. Using the extinction coefficient, it was determined by ultraviolet-visible spectroscopy that the solubility was 0.998 M.

The solubility of all the complexes were similarly determined and tabulated in Table 2.3. The table shows that the solubilities of $Ni(PEt_3)_2Cl_2$ and $Ni(PEt_3)_2Br_2$ were the greatest amongst the six complexes.

Table 2.3. Solubilities of the complexes in CH_2Cl_2.

Compound	Solubility (M) at 20±2°C
$Ni(PEt_3)_2Cl_2$	0.998
$Ni(PEt_3)_2Br_2$	0.709
$Ni(PEt_3)_2I_2$	0.055
$Ni(PPh_3)_2Cl_2$	0.01488
$Ni(PPh_3)_2Br_2$	0.077
$Ni(PPh_3)_2I_2$	0.056495

2.2.7. The relationship of film thickness to the nature of the solvent of the precursor solution.

Solutions of $Ni(PEt_3)_2Cl_2$ in CH_2Cl_2, CH_3COCH_3, $CHCl_3$, CCl_4, and CH_2ClCH_2Cl were made at 0.055±0.005 M. These solutions were spin coated at 1700 rpm. The thickness of the resulting films are given in a bar graph of Figure 2.9 which shows error bars (±0.002 abs. units) that were determined by the difference in intensity of the baselines of the spectra. The order of the solutions in the bar graph is in the order of increasing boiling point (b.p) of the solvent used in the precursor solutions. The boiling points were obtained from the 70th Edition of the CRC Handbook.[32]

Figure 2.9. Film thickness as a function of solvent of solution for $Ni(PEt_3)_2Cl_2$.

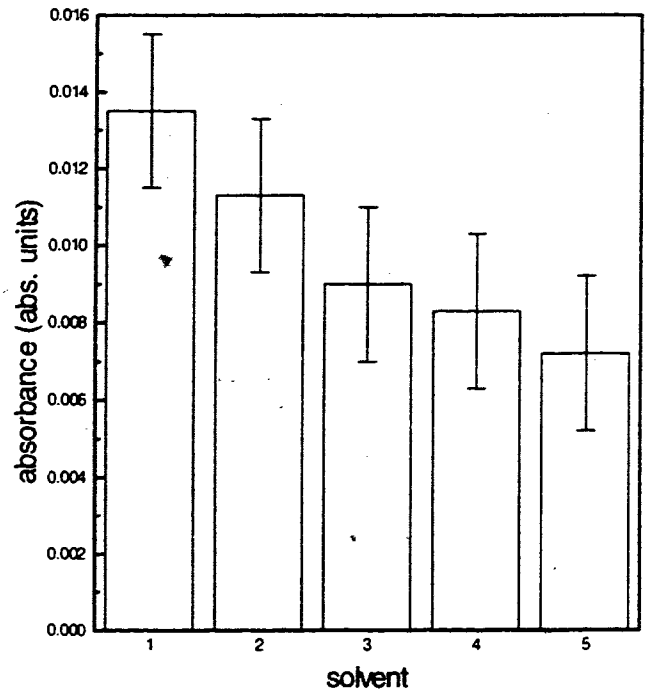

Legend: 1=CH_2Cl_2 (b.p.= 39.8-40.0 °C), 2=CH_3COCH_3 (b.p.= 56.2°C)
3=$CHCl_3$(60.5-61.5 °C), 4= CCl_4(76.7±1.0 °C), 5=CH_2ClCH_2Cl (83 °C)

The same procedure was followed for 0.055±0.005 M solutions of $Ni(PPh_3)_2I_2$ in CH_2Cl_2, CH_3COCH_3, and CH_2ClCH_2Cl. The results are given in the bar graph of figure 2.10.

Figure 2.10. Film thickness as a function of solvent of solution for $Ni(PPh_3)_2I_2$.

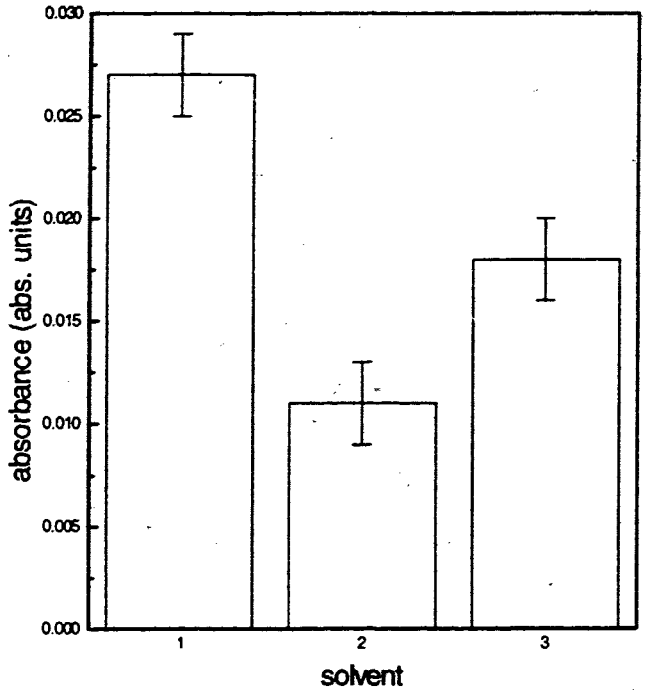

Legend: 1=CH_2Cl_2 (b.p.= 39.8-40.0 °C), 2=CH_3COCH_3 (b.p.= 56.2°C), 3=CH_2ClCH_2Cl (83 °C)

In the case of the $Ni(PEt_3)_2Cl_2$, the solvents which yielded the thickest films in increasing order of thickness were those with the lowest boiling points. The solvents which yielded the thinnest films, had the highest boiling points.

This trend was not found for the films of $Ni(PPh_3)_2I_2$. The use of CH_2Cl_2 (b.p.=39.8-40.0 °C) resulted in the thickest film, however, use of CH_2ClCH_2Cl (83 °C) produced a thicker film than CH_3COCH_3 (b.p.= 56.2°C).

2.2.8. Morphology of the Films.

A film of $Ni(PEt_3)_2Cl_2$ was made by the spin coating method described in section 1.1. The concentration of the precursor solution was 0.018 M of $Ni(PEt_3)_2Cl_2$ in CH_2Cl_2 and the spin speed was 1700 rpm. Examination of the resulting film by light microscopy revealed that the film was crystalline in 85±15% of the area. The measurement of the morphology is a subjective determination that was arrived at after examining numerous different films.

The same experiment was performed for each complex in order that the morphologies of the films as a function of the complex could be examined. The concentration of 0.018 M was selected because it is a concentration within the range that all six nickel complexes are soluble. Furthermore, 0.018 M is of sufficiently high concentration to produce reasonably thick films (section 2.2.3). The spin speed of 1700 rpm was selected because it is a typical speed in the range of speeds which show approximately constant film thickness with varying spin speed (section 2.2.4). Films of the complexes of $Ni(PEt_3)_2Br_2$, $Ni(PEt_3)_2I_2$, $Ni(PPh_3)_2Cl_2$, and $Ni(PPh_3)_2Br_2$ appeared to be crystalline in 50±25% of the area of the film; and films cast from $Ni(PPh_3)_2I_2$ appeared to be crystalline in 10±5% of the area.

Films of all of the complexes were additionally examined when cast at a variety of other speeds between 0 and 4000 rpm. The results found for films cast at 1700 rpm were the same found for films cast at all speeds between 500 and 4000 rpm. And all complexes produced films with 85±15% crystallinity when spin speeds were 50-500 rpm.

2.3. Discussion

The nickel complexes of $Ni(PEt_3)_2X_2$ and $Ni(PPh_3)_2X_2$ (X=Cl, Br, and I) were spin coated into thin films under several different conditions. It was found that the film thicknesses and film morphologies were determined by a combination of concentration of the precursor solution, spin speed, solvent type, and the nature of the metal complex being spin coated. Many of the results will be compared to similar studies made on polymer films.[28, 33-36, 40-49]

2.3.1. Methods of Measurements

The thicknesses of the $Ni(PEt_3)_2X_2$ and $Ni(PPh_3)_2X_2$ films were determined with absorbance infrared spectra of the films. The intensities of the absorbance bands were correlated to measurements of thickness in molecules per Angstrom squared (molecules/$Å^2$) by using a Beer Lambert plot (sections 2.2.2 and 2.5.4). The absorbance bands selected to measure thickness represented the vibrations of the "-PPh_3" and "-PEt_3" ligands. Unfortunately, the "Ni-P" and "Ni-X" vibrations were not monitored because these bands are found in the far infrared region.[17, 25, 26, 29] See Table 2.1 for the list of the infrared absorbance bands used in this thesis.

One of the advantages of using Beer Lambert plots of infrared spectra to determine the thickness of the films is that an average thickness within an area of 7.8 x 10^{15} $Å^2$ was determined. By contrast, the commonly used stylus method[1] and method by interferometry[1], give the thickness measurement for a localized area of a film. The

purpose of the study was to determine trends in film thickness and therefore, an average thickness over a larger area of each film was more useful in making comparisons of film thickness amongst the films.

Another advantage of measuring film thickness by the intensity of the infrared bands is that the resulting measurements were expressed in terms of numbers of molecules rather than in units of length. Thickness measurements obtained by the stylus method and by interferometry, are in units of length, which are the equivalent to units of molecules/$Å^2$ multiplied by the density of the molecules. Measuring film thickness in units of length is not as useful for the film thickness studies of this thesis because the data could not be used to compare the results of the thicknesses of the films made of different complexes. Potential differences in the densities of films made by the different complexes would in that case skew the results of film thickness trends.

The limitation of measuring film thickness with Beer Lambert plots of infrared spectra is that the morphology of the films made for the Beer Lambert plots differ from the morphology of spin coated films. The films made for the Beer Lambert plots cannot be made by spin coating because an indeterminate number of molecules forms the film by this method. The films were instead air dried. It was noted by optical observation of many spin coated and air dried films, that the air dried films were not as smooth as the spin coated films and that they contained more crystals than the spin coated films. The greater number of crystals in the air dried films would have refracted the infrared beams more than the films made by spin coating. Therefore, there is error inherently associated with the method of measuring films using Beer Lambert plots. Fortunately, this

circumstance was consistent among the films of all the complexes so that it was still possible to determine thickness trends amongst the six complexes.

The method of examining the morphologies of the films was by observation through a light microscope. The method is comparable to the method in geology of petrology or petrographic microscopy. Webster's dictionary defines petrography as 'the description and systematic classification of rocks, usually based on microscopic study."[73] For example, petrography is used to determine the degree of crystallinity[74] in a rock from thin slices of the rock sample. Sample of rocks can be holocrystalline, holohyaline, or hypocrystalline, which means the samples are entirely crystalline, entirely glass, or a mixture or crystals and glass respectively.[74] The samples of spin coated films appeared to be classifiable into these three categories. In most cases, however, the samples were hypocrystalline. Films which appeared to be mostly composed of glass, looked very smooth under the microscope. The samples with a greater number of crystals appeared rougher. On a macroscopic level, the films with more crystals had a foggy appearance. The samples which were judged as glassy, reflected colours of the visible spectrum.

2.3.2. The conditions of spin coating which determined the thickness and morphology of the films.

The concentration of the precursor solution, the spin speed of the substrate, and the solvent type of the precursor solution were all tested for their affect upon the thicknesses of the spin coated films of the nickel complexes. In studies of polymer films[6, 10, 26, 28, 33-36], these three variables have been found to play a significant role in determining the film thicknesses of spin coated polymer films. The numerous

investigations of spin coated polymer films are useful as comparisons to this study of spin coated inorganic complexes. A more thorough examination of the relationship between film thickness, and concentration of the precursor solution, spin speed and other factors will be presented by comparing the results to those of polymer films.

Before comparing the properties of the spin coated nickel complex films with the properties of spin coated polymer films, the methods of making spin coated films will be clarified. The polymeric spin coated films described in the literature were produced by pipetting a polymeric solution onto a stationery wafer which was then accelerated to the quoted final spin speed.[26, 28] The spin speeds quoted for the casting of the nickel complex films were the spin speeds that each wafer was spinning at when the solution was pipetted onto the wafer. If the nickel complex solutions had been pipetted onto stationery wafers, evaporation and crystallization would have had the opportunity to occur before spinning started. Furthermore, the acceleration rate of the wafers could not be monitored by the equipment used. Therefore, a controlled experiment was best achieved by spin coating the films on wafers that had already reached their selected spin speed.

In the literature,[33] Damon presented a simple mathematical model (Equation 2.1.) of factors that determine the film thickness of spin coated polymer films. This empirical equation shows that two important variables to affect thickness are spin speed and concentration of the precursor solution.

$$l=kc^{2}\omega^{-a} \qquad (2.1)$$

l=film thickness

k=constant

c=solute concentration

ω=rotation speed

a=0.5

Meyerhofer[34] further investigated Damon's equation and found that when a=0.5 (in $l \alpha \omega^{-a}$), the equation is applicable to systems with a volatile solvent. Furthermore, a is larger than 0.5 for solutions with non volatile solvents (for example a=0.67). Lai[35] also did related work on different solvents and found that for his systems containing volatile solvents, the a value was 0.54, which is very close to 0.50 as found by Damon[33] and Meyerhofer.[34]

In measuring the thicknesses of the films of nickel complexes as a function of concentration of precursor solution, (spin speed ω= 1700 rpm), it was found that film thickness was greater when made from solutions of higher concentration (section 2.2.3). The exact relationship of thickness and concentration of the precursor concentration can be determined by comparing the results to Damon's equation. The equation is generalized to Equation 2.2 for purposes of testing its applicability to spin coated films of inorganic complexes.

$$l = kc^{b}\omega^{-a} \qquad (2.2)$$

b= 2 for polymer films

This equation is further transformed by applying natural logarithms.

$$Ln\ l = Ln\ (kc^{b}\omega^{-a}) \qquad (2.3)$$

$$Ln\ l = Ln\ k + b\ Ln\ c - a\ Ln\ \omega \qquad (2.4)$$

Under conditions of constant spin speed, Equation 2.4 can be simplified to Equation 2.5 where the factors in parentheses are a constant.

$$Ln\ l = b\ Ln\ c + (Ln\ k - a\ Ln\ \omega) \qquad (2.5)$$

By transforming Damon's equation to the format of Equation 2.5, the equation can be used to determine the relationship of thickness to concentration of the precursor solution of the inorganic complexes. The slope of a graph of Ln *l* versus Ln *c* (Ln Absorbance versus Ln Concentration) for each complex yields the corresponding value of *b*. The graph of Ln *l* versus Ln *c* for the spin coated films of $Ni(PEt_3)_2Cl_2$ is given in Figure 2.11. The line on the graph was determined by a linear regression fit. It's value for *b* is 1.92±0.19.

Figure 2.11. Graph of Ln Absorbance vs. Ln Concentration of $Ni(PEt_3)_2Cl_2$

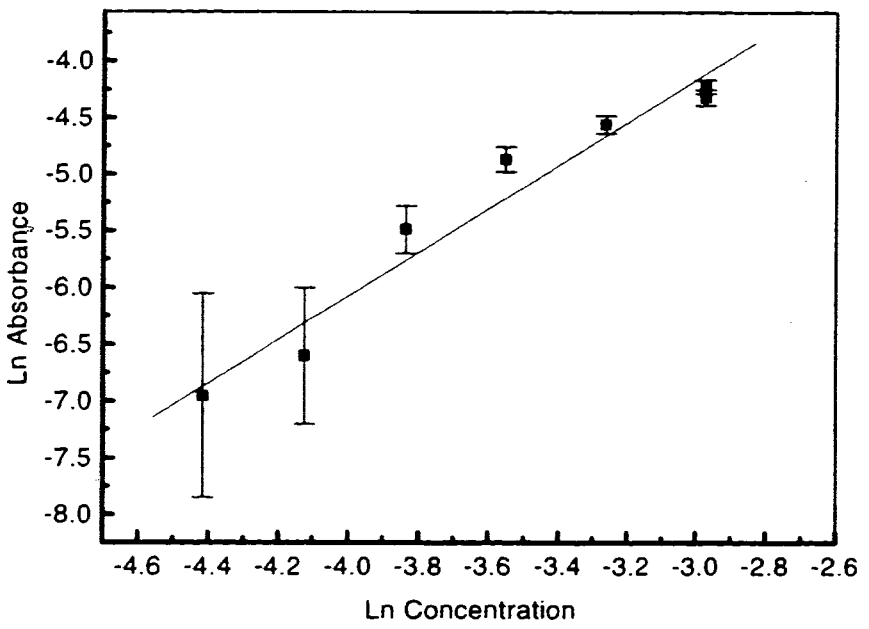

Table 2.4 lists the *b* values of the graphs of Ln Absorbance versus Ln Concentration for all the films of the set of nickel complexes. Except for the film of $Ni(PEt_3)_2Cl_2$, the films had slopes closer to 1.00 than to 2.00 as in the case of polymer films. Therefore for $Ni(PEt_3)_2Br_2$, $Ni(PEt_3)_2I_2$ and $Ni(PPh_3)_2X_2$ (X=Cl, Br, and I), the relationship of film thickness to concentration is approximately $l \alpha c$.

Table 2.4. Slopes of Graphs of Ln absorbance *vs.* Ln concentration

Compound	Slope
$Ni(PEt_3)_2Cl_2$	1.92±0.19
$Ni(PEt_3)_2Br_2$	1.32±0.08
$Ni(PEt_3)_2I_2$	1.15±0.14
$Ni(PPh_3)_2Cl_2$	0.99±0.18
$Ni(PPh_3)_2Br_2$	0.73±0.06
$Ni(PPh_3)_2I_2$	1.05±0.07

The results of spin coating inorganic films at different spin from solutions of constant concentration (0.018 M) were initially graphed as Thickness versus Spin Speed. Figure 2.8 shows the graph for the films of $Ni(PEt_3)_2Cl_2$. The graphs for all six complexes were very similar. The film thicknesses were strongly influenced by the spin speed at speeds of less than 500 rpm; and at speeds of 500-4000 rpm, the resulting thicknesses remained constant.

In order to determine the *a* values of the spin coated films of inorganic complexes, Equation 2.4 was again simplified. Because the films were made from solutions of constant concentration (0.018 M), the factors in parentheses of Equation 2.6 are constant.

$$Ln\ l = -a\ Ln\ \omega + (Ln\ k + b\ Ln\ c) \qquad (2.6)$$

The *a* value for a given complex is derived from the slope of a graph of Ln *l* versus Ln ω. Figure 2.12 is of the graph of Ln *l* versus Ln ω for $Ni(PEt_3)_2Cl_2$. The straight line is made using a linear regression fit. The corresponding *a* value is 0.37±0.05.

Figure 2.12. - Logarithmic Spin Speed Graph of $Ni(PEt_3)_2Cl_2$

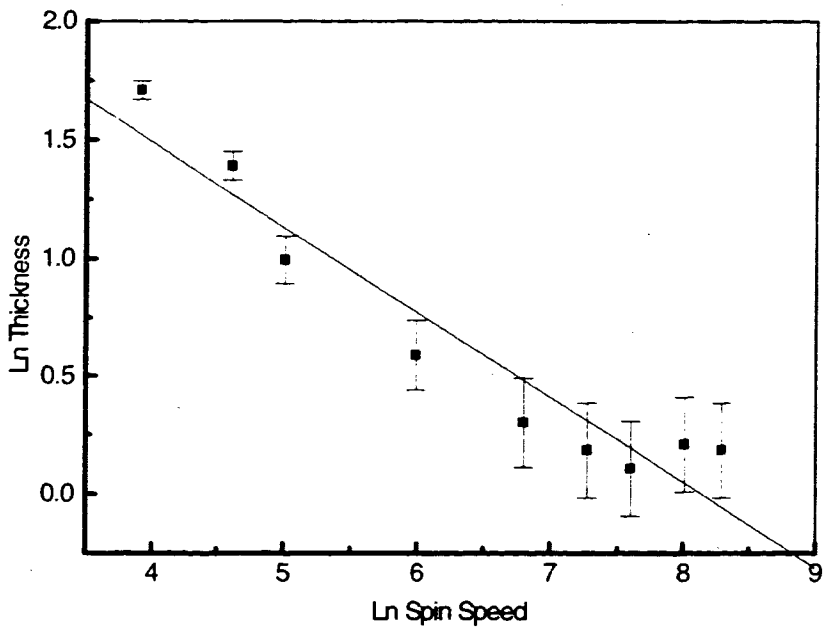

Table 2.5 lists the *a* values found for the films of $Ni(PEt_3)_2X_2$ and $Ni(PPh_3)_2X_2$. The *a* values for the three $Ni(PPh_3)_2X_2$ complexes are in the range of 0.5 to 0.6. In contrast, the films of $Ni(PEt_3)_2X_2$ are instead varied between 0.27 and 0.37. Therefore, the films of the triethylphosphine analogues of the nickel complexes yield films with a greater number of molecules on the surface of the silicon substrate than the films of the triphenylphosphine analogues as a function of spin speed.

Table 2.5. The *a* values of the nickel complexes.

Complex	*a* Values
$Ni(PEt_3)_2Cl_2$	0.37±0.05
$Ni(PEt_3)_2Br_2$	0.37±0.19
$Ni(PEt_3)_2I_2$	0.27±0.13
$Ni(PPh_3)_2Cl_2$	0.57±0.21
$Ni(PPh_3)_2Br_2$	0.47±0.06
$Ni(PPh_3)_2I_2$	0.66±0.10

The logarithmic graphs of the thickness, concentration and spin speed of spin coated inorganic films indicate that film thickness follows the relationships in the generalized version of Damon's equation. To illustrate the fit, a graph of the results of the spin coated films of $Ni(PEt_3)_2Cl_2$ are presented in Figure 2.13. Figure 2.13 is a graph of Ln *l* versus *Ln* $(c^b\omega^{-a})$ where b= 1.92±0.19 and a= 0.37±0.05. The data was fit to a linear regression fit and the dotted lines represent the 95% confidence interval.

Figure 2.13. Graph of Ln l vs. Ln $c^{b}\omega^{a}$ for $Ni(PEt_3)_2Cl_2$.

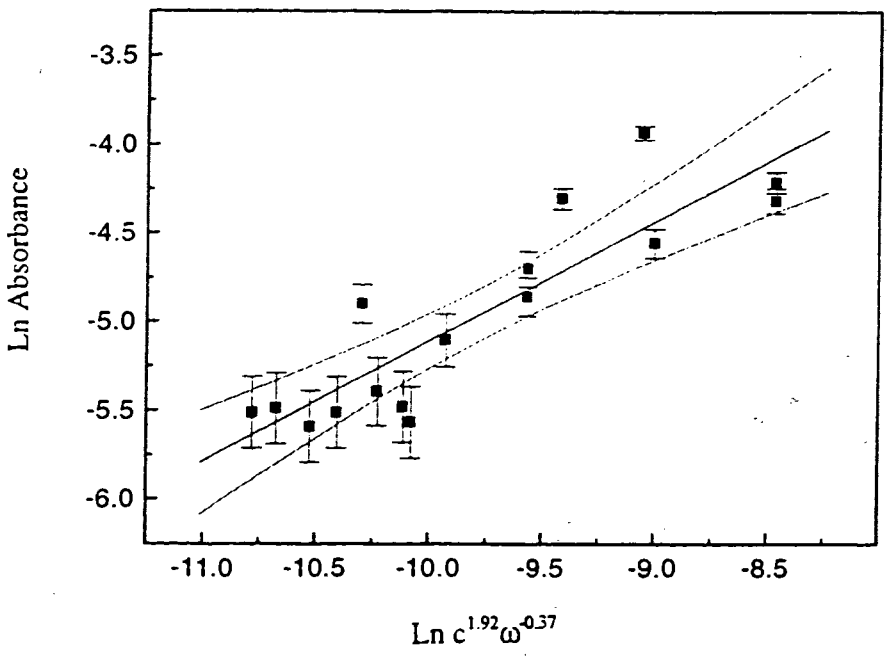

The variables *a, b* and *k* of Damon's generalized equation indicate that there are additional variables which contribute to determining the film thickness. The thickness of spin coated films, whether they be films of polymers or inorganic complexes, is therefore, the product of a combination of factors.

A list of variables affecting the film thickness of spin coated polymer films, is found in the literature. It has been shown, that the value of *a* depends on the volatility of the solvent used in the precursor solution. Solvents of low volatility yield greater values of *a* and hence thinner films than in films made from solutions containing solvents of higher volatility. Other important variables[6, 28, 40, 42, 47] include the viscosity, density, surface tension and vapour pressure of the precursor solution; the wind velocity, humidity and temperature of the surrounding air; and the workpiece temperature, the

nature of the polymer or solute, and the nature of the substrate. These variables are reflected in the values of *a*, *b*, and *k*.

To determine the properties of the solvent of the precursor solution that affect the film thickness of the spin coated films of inorganic complexes, $Ni(PEt_3)_2Cl_2$ and $Ni(PPh_3)_2I_2$ were spin coated from solutions of different solvents. Figures 2.9 and 2.10 of section 2.2.7 indicate the thicknesses of the films when the different solvents were used. It was found that in the case of the five films of $Ni(PEt_3)_2Cl_2$, the order of films from thickest to thinnest matched a trend in the solvents of lowest to highest boiling point (CH_2Cl_2, CH_3COCH_3, $CHCl_3$, CCl_4, and CH_2ClCH_2Cl). In the three solvents that the $Ni(PPh_3)_2I_2$ complex was tested in, the thickest to thinnest films ($Ni(PPh_3)_2I_2$ in CH_2Cl_2, CH_3COCH_3, and CH_2ClCH_2Cl) did not show a matching trend to boiling points, although the solvent that yielded the thickest film (CH_2Cl_2) had the lowest boiling point. Table 2.6 lists literature values of physical properties of the solvents tested. Trends found in this table could not be matched to the order of film thickness of the spin coated films of $Ni(PEt_3)_2Cl_2$ or $Ni(PPh_3)_2I_2$.

Table 2.6. Physical properties of solvents of precursor solutions.[32, 54]

Solvent	Heat of Vap.	Boiling Point	Density 25°C	Viscosity (cp)
CH_2Cl_2	7572 cal/mol	39.8-40.0 °C	1.325 g/ml	0.393 (15 °C)
$CHCl_3$	7501 cal/mol	60.5-61.5 °C	1.4460 g/ml	0.58 (20 °C)
CH_2ClCH_2Cl	7951 cal/mol	83 °C	1.256 g/ml	0.800 (19.4 °C)
CCl_4	8272 cal/mol 7629 cal/mol	76.7±1.0 °C	1.583 g/ml	0.969 (20 °C)
BuOH	10971 cal/mol	117.2 °C	0.8098 g/ml	2.948 (20 °C)

Films made under the same conditions using different complexes, yielded films of different thicknesses. For example the films of $Ni(PPh_3)_2I_2$ and $Ni(PEt_3)_2Cl_2$ were thicker than films of the remaining four complexes. The $Ni(PPh_3)_2I_2$ is the largest molecule out of the series of six complexes and the $Ni(PEt_3)_2Cl_2$ is the smallest. Their geometries are different as well. X-ray analyses and analyses by magnetic susceptibility presented in the literature indicate that the $Ni(PEt_3)_2Cl_2$ has square planar geometry (as do the bromo and iodo analogues)[17, 25, 29, 32] while the $Ni(PPh_3)_2I_2$ has tetrahedral geometry (as do the chloro and bromo analogues).[16, 32, 38] The solubilities for $Ni(PPh_3)_2I_2$ and $Ni(PEt_3)_2Cl_2$ in CH_2Cl_2 (Table 2.3) vary widely too at 0.056 M and 1.00 M respectively (Section 2.2.6). These contrasts support the idea that the thickness of the corresponding films of $Ni(PPh_3)_2I_2$ and $Ni(PEt_3)_2Cl_2$ are thickest for different reasons.

The films of $Ni(PPh_3)_2I_2$ and $Ni(PEt_3)_2Cl_2$ also differed in their morphologies. Upon spin coating, the molecules of the $Ni(PEt_3)_2Cl_2$ readily formed optically visible crystals on the substrate. However, the molecules of the $Ni(PPh_3)_2I_2$ did not. The remaining four nickel complexes sometimes appeared as crystals and sometimes not.

The spin speed of the wafer was also found to affect the morphology of the film. At high spin speeds, most of the solution escaped the wafer because of the strong centrifugal force (see Equation 2.7[39]). Except in the case of $Ni(PEt_3)_2Cl_2$, the quickly formed resultant film appeared amorphous. At low spin speeds (0-500 rpm), the centrifugal force is low and it follows that the liquid solution is forced off relatively slowly. Evaporation increasingly then becomes more important because the solution

remains on the wafer longer. Films dry more slowly affecting the morphology of the resulting film.

$$F=mw^2r \qquad (2.7)$$

F=centrifugal force

m=mass of the solution

w=angular spin velocity

r=radial distance from the axis of the disk rotation

2.4. Conclusion

The ability to control the thickness and the morphology of films produced in the process of spin coating metal complex films is a key factor in successfully applying the technique to industry, particularly for photolithographic applications.

The ideal thickness and morphology of spin coated films of metal complexes is determined by a balance of variables. The empirical relationship of thickness to spin speed and concentration of the precursor solution is given in Damon's equation (Equation 2.2 $l= kc^b\omega^{-a}$). From the spin speed graphs, *a* values ranged from 0.27-0.37 (Table 2.5) for the films of $Ni(PEt_3)_2X_2$ and 0.47-0.66 for the films of $Ni(PEt_3)_2X_2$. However, low spin speeds (less than 500 rpm) are likely to result in films which contain crystals that are optically visible. Amorphous films can still be produced though, depending upon the nature of the complex. For example, the films of the molecule $Ni(PPh_3)_2I_2$ showed a stronger resistance to crystallizing and the films of the $Ni(PEt_3)_2Cl_2$

always appeared crystalline. High precursor solution concentration produced films of greatest thickness as demonstrated by the results in Table 2.2 and Table 2.4. The values of *a*, *b* and *k* reflect other factors that influence film thickness. Some of these factors may include viscosity, density, surface tension and vapour pressure of the precursor solution; the wind velocity, humidity and temperature of the surrounding air; and the workpiece temperature, the nature of the polymer or solute, and the nature of the substrate.

There are different directions for future studies of the film thickness of spin coated films of inorganic complexes. The empirical relationships of films thickness and variables other than spin speed and concentration of the precursor solution could be determined. Also the principles of why Damon's equation is applicable is not fully understood; therefore the application of fundamental physics equations can be explored to develop more sophisticated theories of the dynamics of spin coating inorganic complexes.

2.5. Experimental Section

Silicon wafers were P-type Si(111) and were obtained from Pacific Microelectronics Centre. They were cut into approximately 1x1 cm^2 for the spin coating process. All the chips were cleaned in reagent grade CH_2Cl_2 before spin coating. The spin coating was done with a Laurell Technology Co. spin coater. All of the films were viewed under a Leitz light microscope to assess their quality in terms of crystallinity. Fourier transform infrared (FTIR) spectra were recorded with a Bomen MB-120

spectrophotometer on samples held in an aluminum chamber by steel clips. Ultraviolet-visible spectra measurements were obtained with an HP 8452 diode array spectrophotometer. The viscosity of the nickel complexes solutions were determined at 22°C using a Cannon-Fenske Routine Viscometer (size 35, viscometer #1434). The elemental analyses were carried out at the Micro Analytical facility of Simon Fraser University.

2.5.1. Syntheses of nickel (II) complexes - $Ni(PR_3)_2X_2$

(a) Synthesis of Bis(triethylphosphine)dichloronickel(II) - $Ni(PEt_3)_2Cl_2$

This complex was prepared by the method of Jensen.[13]

To a solution of $NiCl_2 6H_2O$ (0.5016g, 0.002 moles) in ethanol (20 mL), PEt_3 (0.6 mL, 0.004 moles) was added under a nitrogen atmosphere. The mixture was stirred at room temperature for 0.5 hour. The solvent was evaporated under vacuum to afford small red crystals. The crude material was dissolved in a minimum amount of hot ethanol that had been degassed using nitrogen. Upon cooling, red crystals appeared. The product was filtered, washed with cold ethanol and dried under vacuum overnight.

Anal. Calcd. for $C_{12}H_{30}Cl_2NiP_2$: C, 39.61; H, 8.31. Found: C, 39.54; H, 8.27.

(b) Synthesis of Bis(triethylphosphine)dibromonickel(II) - $Ni(PEt_3)_2Br_2$

This complex was prepared by the method of Jensen.[13]

To a solution of $NiBr_2 3H_2O$(0.005 moles, 1.09 g) in ethanol (10 mL), PEt_3 (1.5 mL, 0.01 moles) was added in a nitrogen atmosphere. Crystals appeared instantly. The

solvent was evaporated under vacuum to afford a purple/brown solid. The pure title compound was crystallized from ethanol.

Anal. Calcd. for $C_{12}H_{30}Br_2NiP_2$: C, 31.69; H, 6.65. Found: C, 31.79; H, 6.72.

(c) Synthesis of Bis(triethylphosphine)diiodonickel(II) - $Ni(PEt_3)_2I_2$

This complex was prepared by the method of Jensen.[13]

To a solution of $NiI_2 6H_2O$ (0.005 moles, 2.1 g) in ethanol (15 mL), PEt_3 (1.5 mL, 0.01 moles) was added in a nitrogen atmosphere. Brown crystals were collected from the slurry and dissolved in a minimum of nitrogen bubbled hot ethanol. Upon cooling, brown crystals of the title compound were filtered, washed with cold absolute ethanol, and dried under vacuum.

Anal. Calcd. for $C_{12}H_{30}I_2NiP_2$: C, 26.26; H, 5.51. Found: C, 26.12; H, 5.50.

(d) Synthesis of Bis(triphenylphosphine)dichloronickel(II) - $Ni(PPh_3)_2Cl_2$

This complex was prepared by the method of Venanzi.[12]

Glacial acetic acid (25 mL) was added to $NiCl_2 6H_2O$ (1.19 g, 0.005 moles) dissolved in distilled water (1mL). Triphenylphosphine (2.62 g, 0.01 moles) was dissolved in glacial acetic acid (12.5 mL) by heating gently. The triphenylphosphine containing solution was added to the nickel containing solution and stirred for 24h. The mixture was cooled and the resulting fine blue/grey crystals were filtered and washed with cool glacial acetic acid. The crystals were dissolved in glacial acetic acid with gentle heating and then crystallized. After filtering and washing with cold glacial acetic acid the crystals were dried under vacuum.

Anal. Calcd. for $C_{36}H_{30}Cl_2NiP_2$: C, 66.10; H, 4.62. Found: C, 65.77; H, 4.71.

(e) Synthesis of Bis(triphenylphosphine)dibromonickel(II) - $Ni(PPh_3)_2Br_2$

This complex was prepared by the method of Venanzi.[12]

$NiBr_2 3H_2O$ (1.36 g, 0.005 moles) was dissolved in n-butanol by heating the mixture to the boiling point. A boiling solution of triphenylphosphine (2.62g, 0.01 moles) in n-butanol was added to the nickel solution. Upon cooling there was formation of green crystals which were subsequently filtered and then crystallized from n-butanol. The pure crystals were filtered, washed with cold n-butanol and dried under vacuum overnight.

Anal. Calcd. for $C_{36}H_{30}Br_2NiP_2$: C, 58.19; H, 4.07. Found: C, 57.94; H, 4.30.

(f) Synthesis of Bis(triphenylphosphine)diiodonickel(II) - $Ni(PPh_3)_2I_2$

This complex was prepared by the method of Venanzi.[12]

To a solution of $Ni(NO_3)_2 6H_2O$ (1.5 g, 0.005 moles) in nitrogen bubbled n-butanol (50 mL), finely crushed potassium iodide (2.5 g, 0.015 moles) was added. The mixture was refluxed for two hours under nitrogen. After cooling the mixture to room temperature, unreacted potassium iodide was filtered. The solution was heated to boiling and added to a boiling solution of triphenylphosphine (2.67 g, 0.01 moles) in butanol (35 mL). The final mixture was slowly cooled to room temperature and then put into an ice bath. The dark purple crystals formed were filtered, washed with cold butanol and dried under vacuum overnight.

Anal. Calcd. for $C_{36}H_{30}I_2NiP_2$: C, 51.66; H, 3.61. Found: C, 52.52; H, 3.53.

2.5.2. Film Coating

Thin films of the $Ni(PR_3)_2X_2$ complexes on silicon substrates were prepared by spin coating as illustrated in Figure 1.1.

The procedure to prepare a spin coated film of $Ni(PEt_3)_2Cl_2$ is representative of the preparation of the spin coated films of $Ni(PR_3)_2X_2$. A silicon chip was placed on the spin coater with the polished side of the chip facing up. It was secured with scotch tape on two sides of the chip. After the chip reached the desired speed of 1700 rpm, a solution of $Ni(PEt_3)_2Cl_2$ in CH_2Cl_2 (1 mL of 0.018 M solution) was dispensed onto the spinning silicon chip. The chip was spun until the solvent had evaporated (1-2 minutes) and the resulting $Ni(PEt_3)_2Cl_2$ film appeared dry.

2.5.3. The morphology of the spin coated films.

Sets of spin coated films of $Ni(PEt_3)_2Cl_2$ were observed under an optical microscope to examine the morphology of the film, particularly the degree of crystallinity of the film. One set of films was cast at spin speeds of 50-4000 rpm with a 0.018 M solution, and the other set of films was cast at a constant spin speed of 1700 rpm at from solutions of concentrations of 0.012-0.048 M.

The same procedure was followed for the films of all $Ni(PEt_3)_2X_2$ and $Ni(PPh_3)_2X_2$.

2.5.4. Beer Lambert Plots

The average thickness of films were measured using calibration curves or Beer Lambert plots. The calibration of absorption intensities for $Ni(PEt_3)_2Cl_2$ is an illustrative example. The procedure is described below.

A solution of $Ni(PEt_3)_2Cl_2$ (0.0034 g) was prepared in CH_2Cl_2 (2 mL) and a drop of the solution (3 μL) was dispensed onto a silicon chip. The solvent evaporated, leaving a film of $Ni(PEt_3)_2Cl_2$ on the silicon surface. The area of the film was 7.8×10^{15} Å^2, corresponding to a coverage of 0.5 molecules/Å^2. The infrared spectrum of the entire film was recorded. The same procedure was repeated several times to build up a thicker film. The infrared band at 1037 cm^{-1} was used to plot the calibration curve of absorbance versus film coverage (molecules/Å^2). The slope of this calibration curve (0.00333 absorbance units Å^2/molecule) is the extinction coefficient used to convert band intensity of the infrared spectra of the films, to film thickness in molecules/Å^2. The error bars associated with each data point (±0.002 abs. units) is the uncertainty observed in the difference in baseline intensity of the spectra.

The same procedure was followed for all of the $Ni(PR_3)_2X_2$ complexes. Figures 2.14 to 2.19 are the spectra and the corresponding Beer Lambert plots of the nickel complexes. Table 2.7 lists the extinction coefficients derived from the plots.

Figure 2.14. The Beer Lambert plot of $Ni(PEt_3)_2Cl_2$.

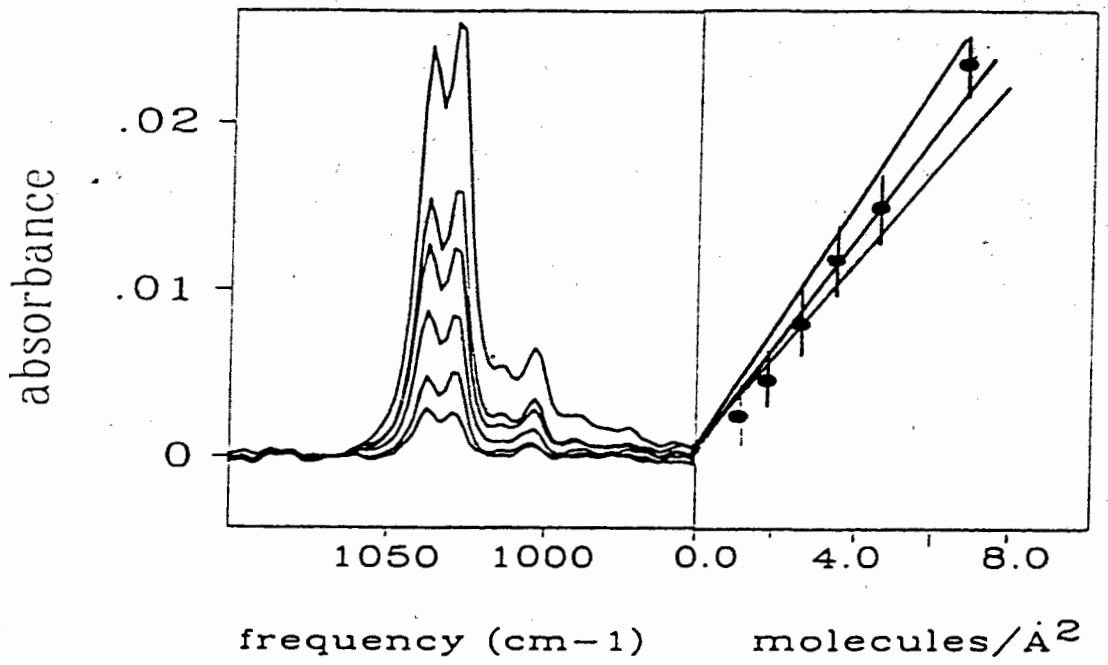

Figure 2.15. The Beer Lambert plot of $Ni(PEt_3)_2Br_2$.

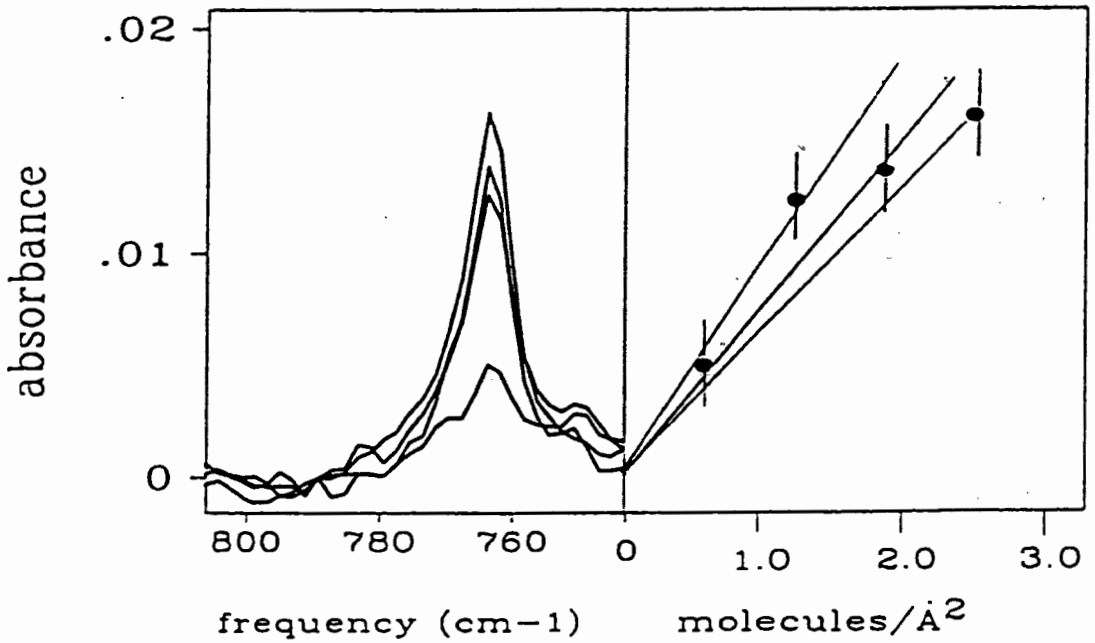

Figure 2.16. The Beer Lambert plot of $Ni(PEt_3)_2I_2$.

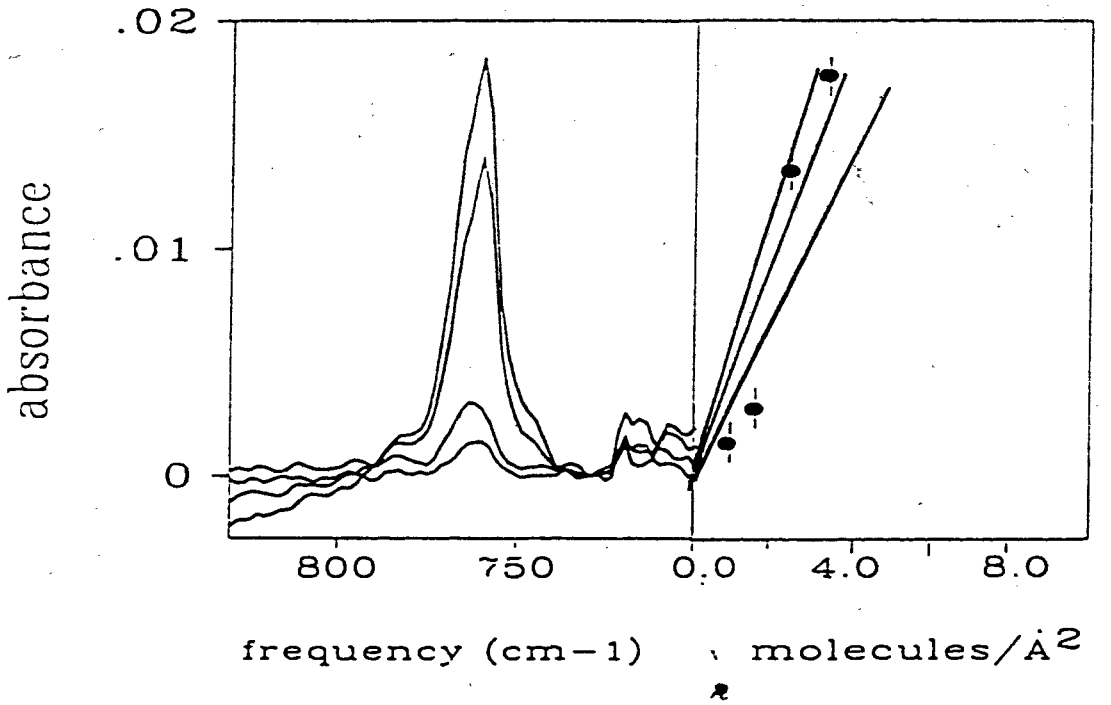

Figure 2.17. The Beer Lambert plot of $Ni(PPh_3)_2Cl_2$

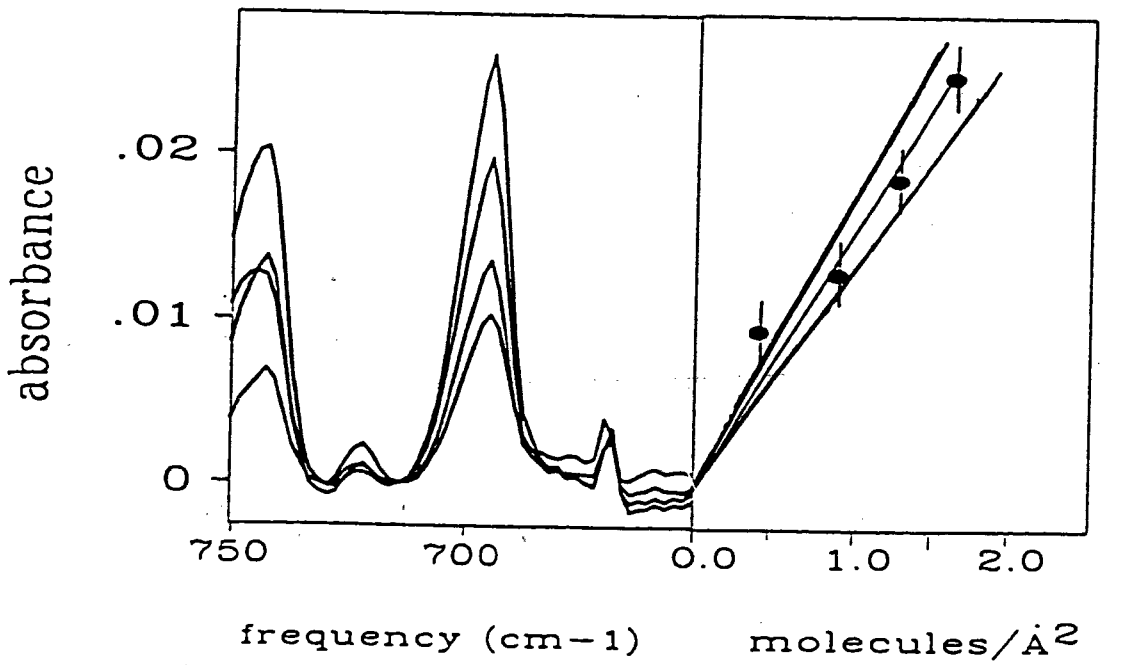

Figure 2.18. The Beer Lambert plot of $Ni(PPh_3)_2Br_2$.

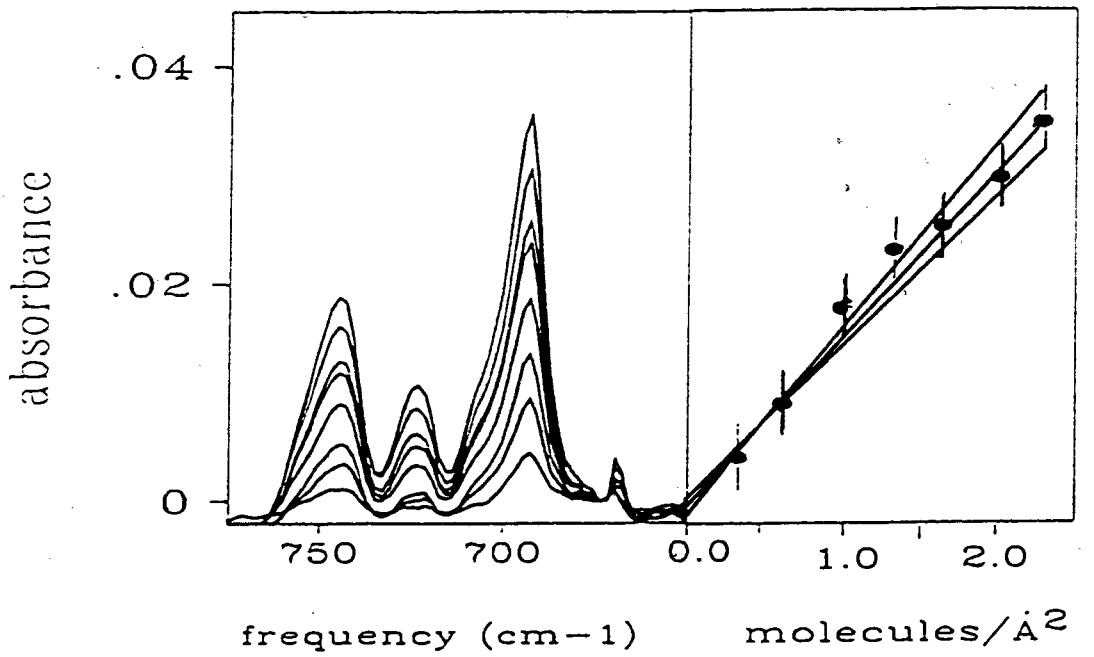

Figure 2.19. The Beer Lambert plot of $Ni(PPh_3)_2I_2$.

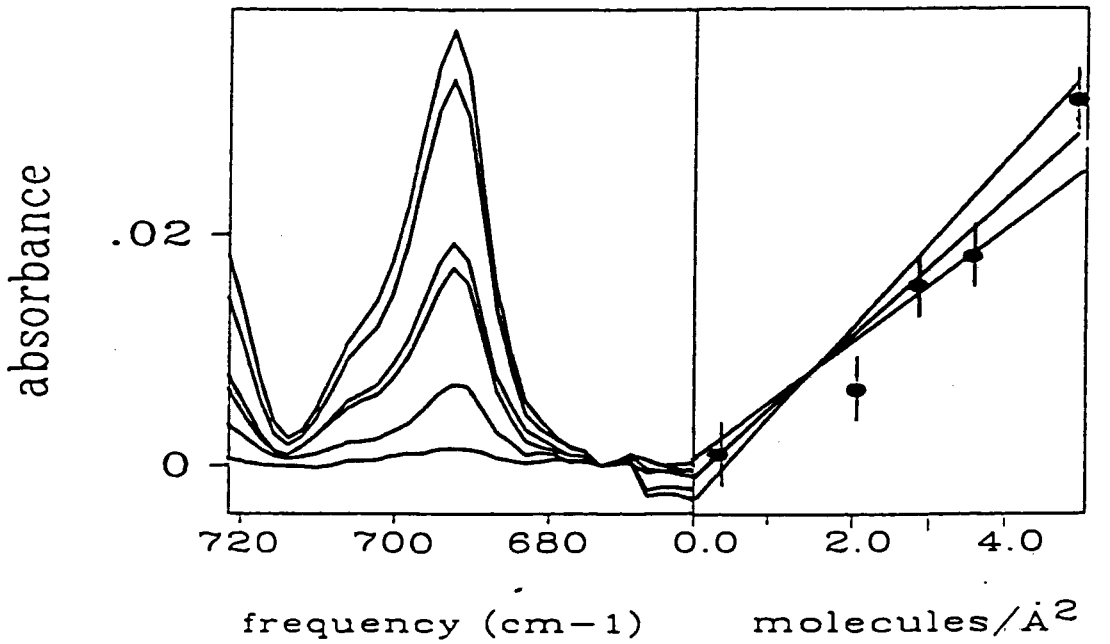

Table 2.7. Extinction coefficients of $Ni(PR_3)_2X_2$.

Compound	Infrared Band	Extinction Coefficient (Absorbance units /(molecules/Å^2))
$Ni(PEt_3)_2Cl_2$	1037 cm^{-1}	0.0032±0.0006
$Ni(PEt_3)_2Br_2$	762 cm^{-1}	0.008±0.002
$Ni(PEt_3)_2I_2$	760 cm^{-1}	0.0050±14
$Ni(PPh_3)_2Cl_2$	696 cm^{-1}	0.0080±13
$Ni(PPh_3)_2Br_2$	692 cm^{-1}	0.0150±.0015
$Ni(PPh_3)_2I_2$	692 cm^{-1}	0.0058±0.0010

2.5.5. The infrared bands of the complexes.

The infrared spectrum of the $Ni(PEt_3)_2Cl_2$ complex in a KBr pellet was acquired to determine the bands due to the complex. The infrared spectra of the spin coated films of $Ni(PEt_3)_2Cl_2$ were compared with the spectrum of the complex in KBr ensuring that the bands were due to the complex and not the solvent trapped in the film. Infrared bands for all of the $Ni(PPh_3)_2X_2$ were identified using the same method.

2.5.6. Films cast from solutions at different concentrations.

More solutions of $Ni(PEt_3)_2Cl_2$ in CH_2Cl_2 were then made at varying concentrations ranging from 0.002 M to 0.045 M. These solutions were each used to spin coat films at 1700 rpm. The resulting films were analyzed by infrared spectroscopy to examine the relationship between film thickness and solution concentration.

This experiment was performed on all six of the $Ni(PR_3)_2X_2$ complexes.

2.5.7. Films cast at different spin speeds.

In the spin speed experiment, a solution of $Ni(PEt_3)_2Cl_2$ in CH_2Cl_2 (0.018 M) was prepared. Portions (1 mL) of this solution were dispensed onto silicon chips spinning at speeds ranging from 50 rpm to 4000 rpm. The resulting films were analyzed by infrared spectroscopy to compare the film thickness with spin speed.

This experiment was performed on all six of the $Ni(PR_3)_2X_2$ complexes.

2.5.8. Films cast from solutions of different solvents.

While the majority of the experiments were carried out using only CH_2Cl_2 as the solution solvent, the $Ni(PEt_3)_2Cl_2$ and $Ni(PPh_3)_2I_2$ complexes were additionally recast into thin films using other solvents to correlate properties of the prepared thin films with physical properties of their mother solution. The $Ni(PEt_3)_2Cl_2$ was cast from solutions of complex in CH_2Cl_2, $CHCl_3$, CH_2ClCH_2Cl, CCl_4, and CH_3COCH_3. The $Ni(PPh_3)_2I_2$ complex was spin coated from solutions of complex in CH_2Cl_2, CH_2ClCH_2Cl, and CH_3COCH_3.

2.5.9. Determination of the saturation concentration using the ultraviolet-visible spectra.

The electronic spectrum of $Ni(PEt_3)_2Cl_2$ in CH_2Cl_2 ($6.39x10^{-3}$ M) was obtained. At λ= 664 nm the extinction coefficient was found at ε=0.926 $mm^{-1}M^{-1}$. A saturated solution of $Ni(PEt_3)_2Cl_2$ in CH_2Cl_2 was then prepared by mixing excess $Ni(PEt_3)_2Cl_2$ in CH_2Cl_2 and then filtering it through tissue paper (Kimwipes). This solution was diluted by pipetting (1 mL) the solution into 10 mL volumetric flask and filling the flask to capacity with CH_2Cl_2. The electronic spectrum of this solution was taken and using the extinction coefficient at λ=664 nm the saturation was determined to be 0.998 M. This procedure was followed for all of the $Ni(PR_3)X_2$ compounds at 20±2°C.

2.5.10. The viscosity of solutions.

The $Ni(PEt_3)_2Cl_2$ complex was dissolved in CH_2Cl_2 (0.03491 M, 1.3160 g/mL) and adjusted to 22°C with a water bath. This solution was drained three times through a Canon Fenske viscometer (size 25, constant of viscometer = 0.001859 cs/sec). The average time through the viscometer was 171.64 seconds which corresponds to a viscosity of 0.3907 centistokes(cs).

The viscosity of each of the complexes dissolved in CH_2Cl_2 and the viscosity of the solvent CH_2Cl_2 were measured and are given in Table 2.8.

Table 2.8. Viscosities of the complexes in CH_2Cl_2.

Compound	Concentration (M)	cs
$Ni(PEt_3)_2Cl_2$	0.03552	0.3907
$Ni(PEt_3)_2Br_2$	0.03421	0.3229
$Ni(PEt_3)_2I_2$	0.03557	0.3210
$Ni(PPh_3)_2Cl_2$	0.02654	0.3242
$Ni(PPh_3)_2Br_2$	0.03491	0.3310
$Ni(PPh_3)_2I_2$	0.03493	0.3269
CH_2Cl_2		0.3199

3. The Photoejection of Halogen Ligands

3.1. Introduction

The purpose of the study in this chapter is to assess the viability of using films of metal complexes with halogen ligands, cast by spin coating, for the photodeposition of metal and metal oxide thin films. It has been shown that metal and metal oxide thin films can be photochemically produced from spin coated metal complex films that contain a variety of different ligands; for example $UO_2(OOCC_5H_{11})_2$, $(COD)Pt(N_3)_2$, and $Ni(EtNC_2H_4NH_2)_2$.[7, 24, 67] Ligands must dissociate and readily escape the film in order to ensure a clean film. The search for precursor films with quick processing times that produce clean films is important in making the process useful for industrial applications.

Nine different films metal complexes with halogen ligands were tested for their photosensitivity. The series of six nickel complexes used in the film quality studies ($Ni(PEt_3)_2X_2$, and $Ni(PPh_3)_2X_2$ where X=Cl, Br, I) were tested and a further three complexes of iron were tested as well ($CpFe(CO)_2X$ where X=Cl, Br, I). The nickel complexes were composed of two halogen ligands while the iron complexes were composed of one halogen ligand. This difference may determine the mechanism by which the dissociated halogens can escape the film.

Ultraviolet spectroscopy, infrared spectroscopy, Auger electron spectroscopy (AES), and energy dispersive spectroscopy (EDS) (see section 1.7 for further explanation of these techniques) were the tools used to study the photochemistry of the films. Electronic spectra of the solutions of the complexes indicated the wavelengths at

maximum absorbency of light. The infrared bands of the phosphine and carbonyl ligands were monitored in between intervals of photolysis. Dissociation of the halogen ligands was not monitored by infrared spectroscopy because the bands due to the vibrations of the metal-halogen bonds are located in the far infrared region. However, Auger electron spectra of the photoproduct films were used to determine if the halogens had been photoejected from the films. The film of photolyzed $CpFe(CO)_2I$ was also analyzed by EDS to complement the analysis done by AES.

3.2. Results

3.2.1. The chemistry of $CpFe(CO)_2Cl$ films.

The ultraviolet spectrum of the $CpFe(CO)_2Cl$ in solution (1.4×10^{-5} M in CH_2Cl_2) contained λ_{max}=340 nm corresponding to ε=1460 cm^{-1} M^{-1}. The literature[60] values were λ_{max}=336 nm and λ_{max}=388 corresponding to ε=935 cm^{-1} M^{-1} and ε=565 cm^{-1} M^{-1}. Pan et al[68] attributed the band at 340 nm to $Fe \rightarrow CO(\pi^*)$.

The infrared spectrum of a spin coated film of $CpFe(CO)_2Cl$ on a silicon wafer was obtained. The wafer was mounted in the infrared chamber as illustrated in Figure 3.7. The most intense infrared bands were identified at 1995 cm^{-1} and 2043 cm^{-1}. From a spectrum of the solution of $CpFe(CO)_2Cl$ in cyclohexane, Alway et al[60] identified the bands at 2005 cm^{-1} and 2050 cm^{-1} as stretching vibrations of the carbon oxygen bond. Ali et al[69] reported that the absorbance bands for $CpFe(CO)_2Cl$ in pyridine are 1990 cm^{-1} and 2045 cm^{-1}.

Experiments were done to test the stability of the spin coated $CpFe(CO)_2Cl$ film before proceeding with photochemical experiments. A film was placed in the chamber in the dark at room temperature for 24 hours. At the end of 24 hours, the infrared bands had not decreased in intensity. This result is consistent with a thermally stable film. A second film was placed in the chamber in the dark at room temperature, and under vacuum. A spectrum was obtained initially and a second spectrum was obtained 10 minutes later. The bands were no longer visible in the second spectrum. The film had sublimed in the infrared chamber under vacuum.

Films of $CpFe(CO)_2Cl$ were photosensitive. A spin coated film of $CpFe(CO)_2Cl$ was mounted in the infrared chamber in a nitrogen atmosphere. Vacuum conditions could not be used due to the sublimation problem. The initial infrared spectrum was obtained, followed by a 10 minute exposure to light from a mercury lamp. Another spectrum was then obtained and the experiment proceeded with alternating exposures to light energy, and spectral analysis at 30, 55, 85, 120 and 270 minutes of photolysis (see Figure 3.1).

Figure 3.1 Spectra of the film of $CpFe(CO)_2Cl$ after 0, 85 and 270 minutes of photolysis.

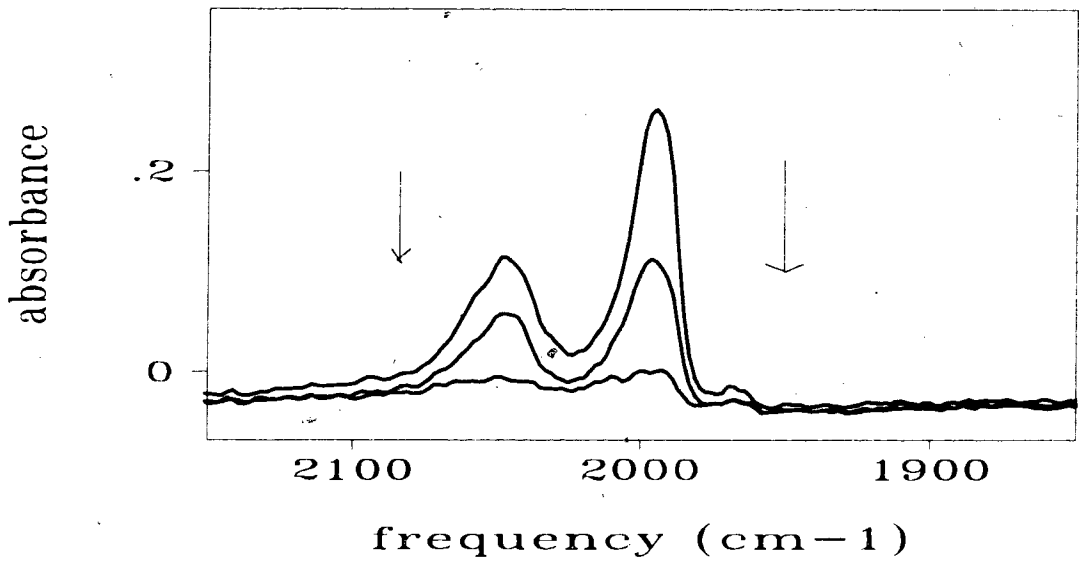

The experiment continued until the infrared bands were no longer visible (half life of 80±15 minutes). An infrared spectrum without any bands visible is consistent with either an elemental iron film, an iron iodide film or an iron oxide film.

Elemental ratios of the photolyzed film were determined using AES (Table 3.1 and 3.2). The error associated with the Auger results was derived from the amount of noise in the spectra. For example, the energy band at 703 eV corresponds to the amount of iron detected. The length of the band is 18.4±1.0 cm which accounts for 18.4±1.5% of the elemental composition. The ±1.0 cm is the measurement of the noise of the spectrum.

Table 3.1. AES analysis (trial 1) of the photolyzed film of $CpFe(CO)_2Cl$.

Element	Initial	10 sec sputter	30 sec sputter
Fe	18.4±1.5%	33±2%	35.5±1.7%
Cl	23.8±0.4%	32±5%	26.4±0.4%
O	21.5±0.8%	22.7±1.1%	26.5±1.2%
C	36±2%	11±3%	11±3%
Fe:Cl	1:1.29	1:0.988	1:0.746

Table 3.2. AES analysis (trial 2) of the photolyzed film of $CpFe(CO)_2Cl$.

Element	Initial	5 sec sputter	15 sec sputter	25 sec sputter
Fe	18±2%	25±2%	34±3%	34±3%
Cl	21.4±0.8%	36.0±1.3%	35.0±1.3%	34.6±1.3%
O	25±3%	21±2%	21.2±1.2%	22.1±1.2%
C	34±6%	16±6%	9±5%	9±5%
Fe:Cl	1:1.13	1:1.42	1:1.01	1:1.01

The spectra were taken before and after sputtering which removes some of the top layers of the film, particularly any carbon contamination. Tables 3.4 and 3.5 show that sputtering resulted in lower carbon percentages in the film (36±2% before sputtering and 11±3% after sputtering).

This data is consistent with the overall reaction in Equation 3.1. The associated proposed mechanism is given in Equation 3.2-3.4. Equation 3.2 is analogous to the

photochemical reaction of $CpFe(CO)_2Cl$ in solution, proposed by Alway et al.[60] In this reaction, the $CpFe(CO)_2Cl$ photochemically loses one carbonyl ligand. The infrared evidence of the photolyzed film shows loss all of the carbonyl ligands. The ratio of the Fe:O:Cl is approximately 1:1:1 throughout in all of the Auger spectra taken.

$$\tfrac{1}{2}\,O_2 + CpFe(CO)_2Cl \xrightarrow{h\nu} FeOCl + [Cp] + 2\,CO(g) \qquad (3.1)$$

$$CpFe(CO)_2Cl \xrightarrow{h\nu} CpFe(CO)Cl + CO(g) \qquad (3.2a)$$

$$CpFe(CO)Cl \rightarrow FeCl + Cp + CO(g) \qquad (3.2b)$$

$$FeCl + \tfrac{1}{2}\,O_2 \rightarrow FeOCl \qquad (3.2c)$$

3.2.2. The chemistry of $CpFe(CO)_2Br$ films.

The complex $CpFe(CO)_2Br$ was not very soluble in CH_2Cl_2 and therefore CH_3CN was used as the solvent in all of the experiments with $CpFe(CO)_2Br$.

The ultraviolet spectrum of the $CpFe(CO)_2Br$ (1.4×10^{-5} M in CH_3CN) contained λ_{max}=350 nm and λ_{max}=394 nm corresponding to ε=1900 $cm^{-1}\,M^{-1}$ and ε=1260 $cm^{-1}\,M^{-1}$ respectively. Ultraviolet results found in the literature[60] were λ_{max}=350 nm and λ_{max}=386 nm corresponding to ε=1028 $cm^{-1}\,M^{-1}$ and ε=700 $cm^{-1}\,M^{-1}$. Pan et al[68] attributed the band at 350 nm to $Fe \rightarrow CO(\pi^*)$.

Analogous to the films of $CpFe(CO)_2Cl$, the spin coated films of $CpFe(CO)_2Br$ were found to be thermally stable and were found to sublime when under vacuum. The

most intense bands of the infrared of the films were 1989 cm^{-1}(shoulder), 2000 cm^{-1} (strong), and 2039 cm^{-1} (strong). Alway et al[60] the infrared bands for $CpFe(CO)_2Br$ at 2003 cm^{-1} and 2045 cm^{-1} corresponding to carbonyl stretching vibrations. Ali et al[69] reported the infrared bands at 1993 cm^{-1} and 2043 cm^{-1}.

The procedure followed for the photolysis of the $CpFe(CO)_2Br$ was the procedure followed for the $CpFe(CO)_2Cl$. Spectra were taken after 9, 17, 28, 36, 47, 62 minutes of photolysis (see Figure 3.2). The half life represented by the decrease in intensity of the infrared bands was 17±3 minutes.

Figure 3.2. Spectra of $CpFe(CO)_2Br$ after 0, 17 and 62 minutes of photolysis.

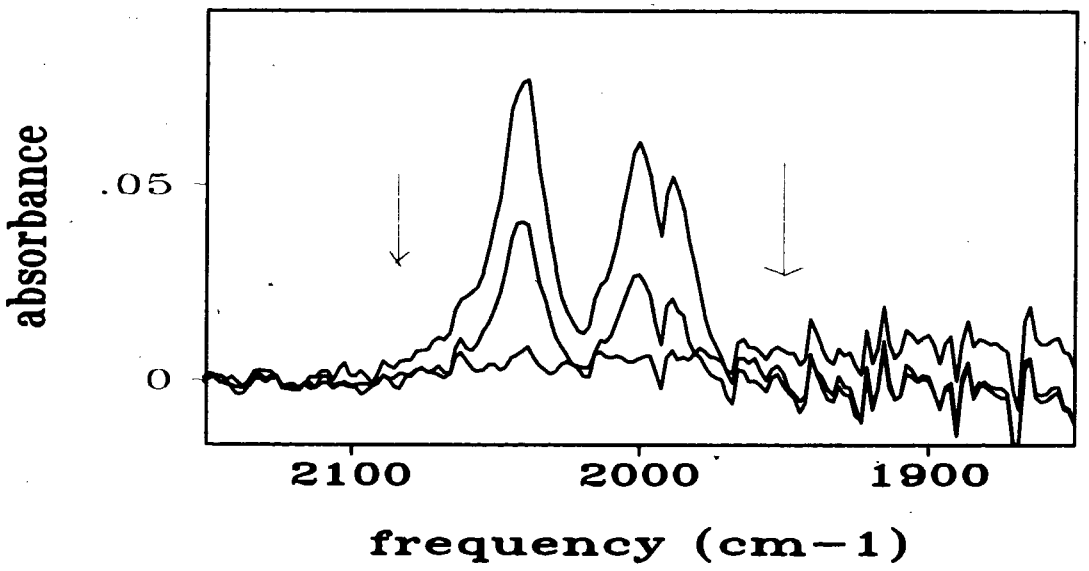

The Auger results of the film of photolyzed $CpFe(CO)_2Br$ (Table 3.3) showed the same results as the film of photolyzed $CpFe(CO)_2Cl$. The amount of carbon decreased from 41±11% to 23±7% after 25 seconds of sputtering and was therefore assigned to carbon contamination. The halogen did not escape the film, indicating that the halogen was a part of the new iron complex or that the dissociated halogen was trapped in the film.

Table 3.3. AES analysis of the photolyzed film of $CpFe(CO)_2Br$.

Element	Initial	5 sec sputter	15 sec sputter
Fe	18±5%	29±7%	31±5%
Br	20±4%	26±5%	22.4±1.7%
O	19±4%	22±4%	24±3%
C	41±11%	22±8%	23±7%
Fe:Br	1:1.1	1:0.88	1:0.70

The overall reaction which is consistent with the data is given in Equations 3.4a-3.4c. The mechanism associated with the reaction is given in Equations 3.4a-3.4c.

$$\tfrac{1}{2}O_2 + CpFe(CO)_2Br \xrightarrow{h\nu} FeOBr + [Cp] + 2\,CO(g) \qquad (3.3)$$

$$CpFe(CO)_2Br \xrightarrow{h\nu} CpFe(CO)Br + CO(g) \qquad (3.4a)$$

$$CpFe(CO)Br \rightarrow FeBr + [Cp] + CO(g) \qquad (3.4b)$$

$$FeBr + \tfrac{1}{2}\,O_2 \rightarrow FeOBr \qquad (3.4c)$$

3.2.3. The chemistry of $CpFe(CO)_2I$ films.

The ultraviolet spectrum of $CpFe(CO)_2I$ (1.4×10^{-5} M in CH_2Cl_2) contained λ_{max}=336 nm corresponding to ε=4390 $cm^{-1}M^{-1}$. The values found in the literature[60] of the ultraviolet spectra are λ_{max}=342 nm corresponding to ε=2090 $cm^{-1}M^{-1}$. Pan et al[68] attributed the band to $Fe \rightarrow CO(\pi^*)$.

Analogous to the films of $CpFe(CO)_2Cl$, the spin coated films of $CpFe(CO)_2I$ were found to be thermally stable and were found to sublime when under vacuum. The most intense bands of the infrared of the films were 1973 cm^{-1}, and 2043 cm^{-1}. Alway et al[60] identified the infrared bands for $CpFe(CO)_2I$ as ν(CO) 2005 cm^{-1} (strong) and ν(CO) 2038 cm^{-1} (strong).

The procedure followed for the photolysis of $CpFe(CO)_2Cl$ was the procedure followed for the photolysis of $CpFe(CO)_2I$. Infrared spectra were taken after 0, 15, 40, 75, 90, and 720 minutes of photolysis. Figure 3.3 shows the decrease in intensity of the bands of the carbonyl stretches. The half life was 120 ± 20 minutes.

Figure 3.3. Photolysis of $CpFe(CO)_2I$ after 0, 90 720 minutes of photolysis.

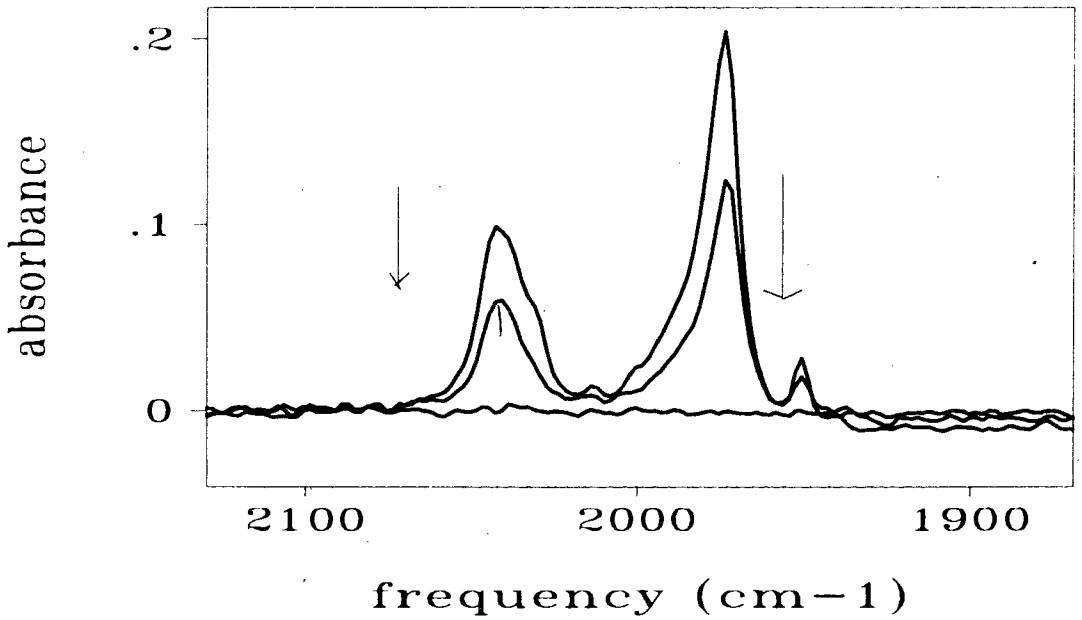

Elemental ratios of the final film were obtained by both EDS and AES. The EDS results are listed in Table 3.4. The EDS analysis was necessary to determine the Fe:I ratio. The reported error of the EDS data (±6%) is the error derived from the calibration

of the EDS instrument. The results show that the photolyzed film contained a negligible amount of iodine (<1.5% iodine). In the Auger results, the signal at 510 eV can be experimentally due to iodine or oxygen; however, because the EDS results indicate that there is virtually no iodine remaining in the film, the signal at 510 eV of the AES was treated as being entirely due to a signal of oxygen Auger electrons from the film. The AES results are in Table 3.5.

Table 3.4. The EDS results of the film of photolyzed $CpFe(CO)_2I$.

Element	Location #1	Location #2	Location #3
Atomic Percent Fe	100±6	100±6	99±6
Atomic Percent I	0.43±0.03	0.08±0.01	1.23±0.07
Fe:I Ratio	232:1	1250:1	80.3:1

Table 3.5. The Auger results of the film of photolyzed $CpFe(CO)_2I$.

Element	Initial	5 sec sputter	15 sec. sputter
Fe	23±10%	37±4%	43±11%
O	33±5%	37±4%	37±8%
C	43±14%	25±12%	18±14%
Fe:O	1:1.4	1:1.1	1:0.85

The Auger results indicate that there was carbon remaining in the film. It could be a result of contamination from the environment, or it could be due to some of the carbon

from the cyclopentadienyl ligand which had not escaped the film product which had not escaped the film after dissociating.

Before sputtering, the Fe:O ratio found in the Auger results, was 1.0:1.4 and after sputtering, the results show that there is less oxygen as a function of sputtering time. Possible explanations are that the sputtering activity preferentially ejects the oxygen atoms from the film; or that when the sputtering reaches the level of the film-substrate interface, there is different chemistry than in the bulk film. The photolysis of the $CpFe(CO)_2I$ complex may result in the formation of an oxide or a combination of oxides of iron. By approximating the Fe:O ratio to be 1:1, the overall reaction that is consistent with the data is given in Equation 3.5. The associated mechanism is given in 3.6a-3.6c.

$$\tfrac{1}{2}\, O_2(g) + CpFe(CO)_2I \xrightarrow{h\nu} FeO + [Cp] + \tfrac{1}{2}\, I_2 + 2\, CO(g) \qquad (3.5)$$

$$CpFe(CO)_2I \xrightarrow{h\nu} CpFe(CO)I + CO(g) \qquad (3.6a)$$

$$CpFe(CO)I \rightarrow FeI + [Cp] + CO(g) \qquad (3.6b)$$

$$FeI + \tfrac{1}{2}O_2 \rightarrow FeO + \tfrac{1}{2}\text{ "I"} \qquad (3.6c)$$

3.2.4. The chemistry of $Ni(PEt_3)_2Br_2$ films.

The sequence of the presentation of results for the films of nickel complexes begins with the results for the film of $Ni(PEt_3)_2Br_2$ and $NiBr_2$. The AES results of the $NiBr_2$ film serve as a useful comparison to the AES results of the film of photolyzed $Ni(PEt_3)_2Cl_2$.

The ultraviolet spectrum of the $Ni(PEt_3)_2Br_2$ (1.93×10^{-5} M and 4.85×10^{-3} M in CH_2Cl_2) contained λ_{max}=280 nm, λ_{max}=396 nm and λ_{max}=538 nm corresponding to ε=5400 cm^{-1} M^{-1}, ε=7800 cm^{-1} M^{-1} and ε=200 cm^{-1} M^{-1} respectively. Giacometti et al[72] attribute the band at 280 nm as a ligand to metal charge transfer associated with the phosphine ligands. They attribute the band at 396 nm as ligand to metal charge transfer of the bromine ligand.

The infrared spectrum of a spin coated film of $Ni(PEt_3)_2Br_2$ on a silicon wafer was obtained. The wafer was mounted in the infrared chamber as illustrated in Figure 3.7. The most intense infrared bands were identified at $\rho(CH_2)$[27] 727 cm^{-1}(strong), $\rho(CH_2)$[27] 764 cm^{-1}(strong), and $\nu(PC)$[27] 1034 cm^{-1}(strong).

Experiments were done to test the stability of the spin coated films of $Ni(PEt_3)_2Br_2$ before proceeding with the photochemical experiments. A spin coated film of $Ni(PEt_3)_2Br_2$ precursor sublimed within 10 minutes of being mounted in the infrared chamber under vacuum conditions. When the film was monitored in the dark, at room temperature, the bands of the infrared spectra decreased in intensity with a half life of 260±30 hours, indicating thermal reactivity.

A spin coated film of $Ni(PEt_3)_2Br_2$ in air was photolyzed by water filtered light from a mercury lamp by the same method used for the films of iron complexes. A

spectrum was obtained after 0, 20, 90, 150, 210, 310, and 1750 minutes of photolysis (half life of 240±30 minutes). Infrared bands decreased until they were no longer visible which is consistent with a film of nickel, nickel oxide or nickel bromide. Figure 3.4 shows the spectra of the film as it is progressing through photolysis. It was observed that the photolyzed film was deliquescent.

Figure 3.4: The infrared spectra of the photolysis of $Ni(PEt_3)_2Br_2$

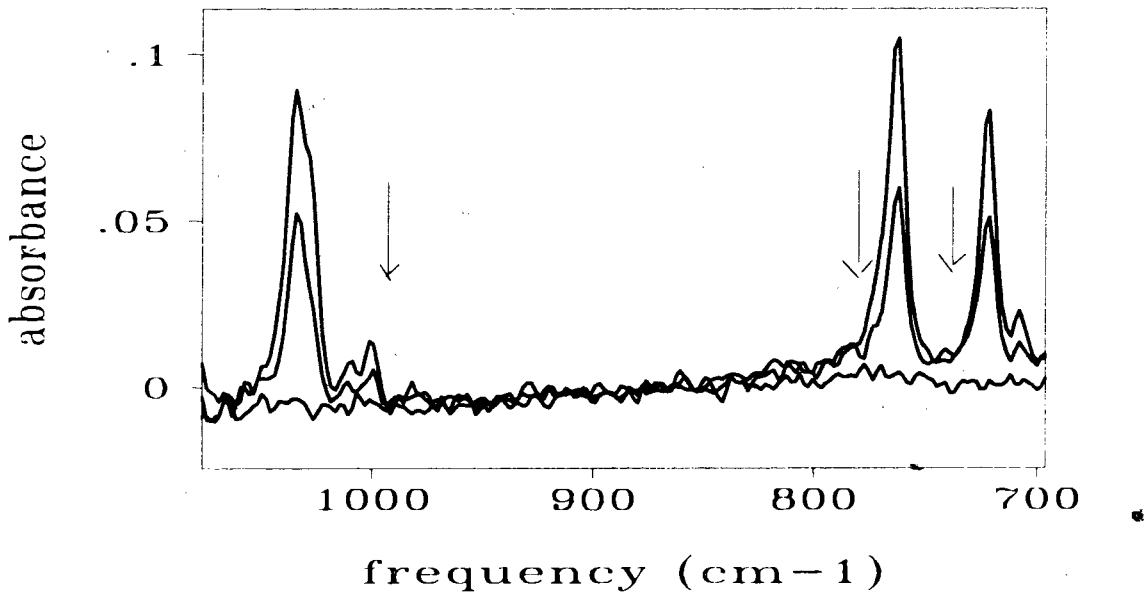

Because $NiBr_2$ is also to be deliquescent, a film of $NiBr_2$ was prepared to compare with the film photolyzed from the $Ni(PEt_3)_2Br_2$ film. The $NiBr_2$ film could not be made by spin coating because the process of spin coating resulted in a wet film. The film was made by heating a silicon chip and dispensing a solution of $NiBr_2$ in CH_2Cl_2 onto it and then letting it air dry.

The AES results (Table 3.6) of the prepared $NiBr_2$ film show that before sputtering there was more bromine than nickel (29±15% and 5.7±1.9% respectively) and there was

carbon and oxygen contamination (54±4% and 10.0±1.3% respectively). After 20 seconds of sputtering, the ratio of Ni:Br went from Ni:Br=1:5.2 to Ni:Br=1:2.0. Therefore, in the AES results, the relative amount of bromine had decreased compared to the relative amount of nickel after sputtering.

Table 3.6: AES analysis of the $NiBr_2$ film.

Element	Initial	10-sec. sputter	20 sec. sputter
Ni	5.7±1.9%	22±5%	24±5%
Br	29±15%	46±14%	48±16%
O	10.0±1.3%	9±2%	8±2%
C	54±4%	21±5%	19±5%

Table 3.7: AES results for the film derived from $Ni(PEt_3)_2Br_2$.

Element	Initial	10-sec. sputter	30-sec. sputter
Ni	16±2%	32±5%	37±5%
Br	41±7%	26±15%	17±12%
P	0.5±0.5%	5.9±1.0%	7.7±1.4%
O	35.6±1.4%	3.8±1.0%	1.3±0.9%
C	6.9±0.4%	32±3%	35±4%

The AES results of the film photolyzed from $Ni(PEt_3)_2Br_2$ (Table 3.7), indicated that bromine was present in the film. Before sputtering the Ni:Br ratio was 1:2.6; after 10 seconds of sputtering, the ratio went to 1:0.81; and after 30 seconds of sputtering, the

ratio went to 1:0.47. Therefore, the sample would have reached a Ni:Br ratio of 1:2 at a sputtering time of less than 10 seconds. It should be noted that the film of the prepared $NiBr_2$ film was much thicker than the spin coated film. After 30 seconds of sputtering, the Auger electrons from the $NiBr_2$ film may still have been ejected from atoms in the bulk film which gave Ni:Br ratios of approximately 1:2. In the thinner photolyzed film, the sputtering reached the interface quickly which accounts for the changing environment at the different sputtering times. The proposed chemical reaction is given in Equation 3.7. The phosphine ligands photodissociate thereby photodepositing a film of $NiBr_2$

$$Ni(PEt_3)_2Br_2 \xrightarrow{h\nu} NiBr_2 + [2\ PEt_3]$$

3.2.5. The chemistry of $Ni(PEt_3)_2Cl_2$ films.

The ultraviolet spectrum of the $Ni(PEt_3)_2Cl_2$ (2.06×10^{-5} M and 6.67×10^{-3} M in CH_2Cl_2) contained λ_{max}=274 nm, λ_{max}=370 nm and λ_{max}=494 nm corresponding to ε=1400 cm^{-1} M^{-1}, ε=10 000 cm^{-1} M^{-1} and ε=200 cm^{-1} M^{-1} respectively. Giacometti et al[27] attribute the band at 274 nm as a ligand to metal charge transfer associated with the phosphine ligands. They attribute the band at 370 nm as ligand to metal charge transfer of the chlorine ligand.

The most intense infrared bands of the films were 727 cm^{-1} (strong), 764 cm^{-1} (strong), 1034 cm^{-1}(strong). The infrared bands for $Ni(PEt_3)_2Cl_2$ were quoted and identified by Courssmaker et al were $\rho(CH_2)$[27] 721 cm^{-1}(strong), $\rho(CH_2)$[27] 762

cm^{-1}(strong), and $\nu(PC)$[27] 1034 cm^{-1}(strong).

Analogous to the films of $Ni(PEt_3)_2Br_2$, the spin coated films of $Ni(PEt_3)_2Cl_2$ were found to be thermally reactive with a half life of 22±4 hours. The films also were found to sublime when under vacuum.

The procedure followed for the photolysis of the $Ni(PEt_3)_2Cl_2$ was the same as the procedure followed for the $Ni(PEt_3)_2Br_2$. Spectra were taken after 0, 30, 120, 300, and 1200 minutes of photolysis. The half life represented by the decrease in intensity of the infrared bands was 100±20 minutes.

The Auger results of the film of photolyzed $Ni(PEt_3)_2Cl_2$ were similar to the results of the film of photolyzed $Ni(PEt_3)_2Br_2$. The amount of carbon decreased from 55±14% to 29±8% after 25 seconds of sputtering and was assigned to carbon contamination. The AES spectrum of the $NiBr_2$ demonstrated that carbon contamination can be significant and that it is most significant before sputtering. The halogen did not escape the film (14 and 16%). This indicates that the halogen was a part of the new iron complex or that the dissociated halogen was trapped in the film. The average Ni:P ratio decreased from a theoretical 1:2 in the film of $Ni(PEt_3)_2Cl_2$ to 1:0.6 of the photolyzed film. This is complemented with the infrared spectrum of the photoproduct in which bands due to phosphine ligands were not visible. The phosphine ligands had dissociated from the nickel complex and escaped the film.

Table 3.8: AES results of photolyzed $Ni(PEt_3)_2Cl_2$.

Element	Initial	5 sec. sputter
Ni	9±3%	21±7%
Cl	14.1±1.5%	16±2%
P	5±2%	14±4%
O	17.0±1.0%	19±3%
C	55±14%	29±8%

The chemical reaction consistent with the data is given in equation 3.8. The phosphine ligands photodissociate thereby photodepositing a film of $NiCl_2$.

$$Ni(PEt_3)_2Cl_2 \xrightarrow{h\nu} NiCl_2 + [2\ PEt_3] \qquad (3.8)$$

3.2.6. The chemistry of the $Ni(PEt_3)_2I_2$ films.

The interpretation of the photolysis experiments of the $Ni(PEt_3)_2I_2$ film was ambiguous. The low solubility of $Ni(PEt_3)_2I_2$ in CH_2Cl_2 resulted in thinner films then was achieved for the films of the $Ni(PEt_3)_2Cl_2$ and $Ni(PEt_3)_2Br_2$. The resulting lower signal to noise ratio of the infrared spectra then made measurements difficult to interpret. It was consequently more difficult to determine if the film was reacting photochemically and thermally; or if it was only reacting thermally .

3.2.7. The chemistry of the $Ni(PPh_3)_2Cl_2$ films.

The ultraviolet spectrum of the $Ni(PPh_3)_2Cl_2$ (1.54×10^{-5} M and 6.02×10^{-3} M in CH_2Cl_2) contained λ_{max}=262 nm, λ_{max}=350 nm and λ_{max}=520 nm corresponding to ε=24000 cm^{-1} M^{-1}, ε=570 cm^{-1} M^{-1} and ε=330 cm^{-1} M^{-1} respectively. Giacometti et al[9] attribute the band at 262 nm as a ligand to metal charge transfer associated with the phosphine ligands.

The infrared spectrum of the spin coated film of $Ni(PPh_3)_2Cl_2$ was obtained and the most intense bands were identified. Bands at 692 cm^{-1} (strong), and 746 cm^{-1} (strong) correspond to vibrations in the phenyl rings.[56, 66] The band at 1095 cm^{-1} (medium) corresponds to phosphorus carbon bending.[56,66]

The tests for the stability of the films were the same as those described in section 3.2.4 for the film of $Ni(PEt_3)_2Br_2$. The film of the $Ni(PPh_3)_2Cl_2$ thermally reacted when left at room temperature in the dark. The thermal reaction resulted in a spectrum which contained bands at 542 cm^{-1}(strong), 692 cm^{-1}(medium), 746 cm^{-1}(medium), and 1095 cm^{-1} (medium) and 724 cm^{-1} (strong). The half life of the thermal reaction was 230±30 hours. The film sublimed under vacuum and therefore subsequent experiments were performed in air.

By the same method described for previous films, the infrared spectra of the films was obtained throughout the photolysis by water filtered light from a mercury lamp. Spectra were obtained at 0, 7, 32, 72, 130, 190, and 1070 minutes. The half life of the photochemical reaction was 120±20 minutes. The photoproduct of the film of

$Ni(PPh_3)_2Cl_2$, was not a metal, metal chloride, or metal oxide film. The product infrared spectrum contained bands at 542 cm^{-1} (strong), 692 cm^{-1} (strong), 746 cm^{-1} (medium), and 724 cm^{-1}(strong). Figure 3.5 shows spectra of the film spin coated from $Ni(PPh_3)_2Br_2$ during the photolysis.

Figure 3.5: The photolysis of $Ni(PPh_3)_2Cl_2$.

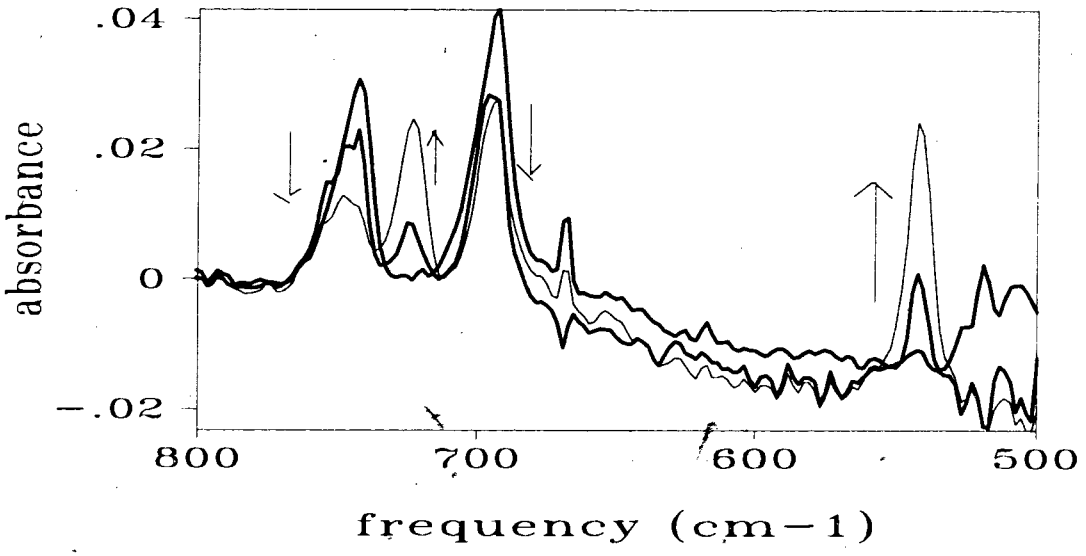

Jensen et al[66] recorded the infrared spectrum of the free PPh_3 and $OPPH_3$ molecules. The spectrum of the PPh_3 contained bands at 695 cm^{-1} (strong) and 747 cm^{-1} (medium); and the spectrum of the $OPPH_3$ molecule contained bands at 540 cm^{-1}(very strong), 690 cm^{-1} (strong), 720 cm^{-1} (strong) and 740 cm^{-1} (medium).[11] Jensen et al[66] identified the band at 540 cm^{-1} (very strong) as corresponding to the asymmetric stretch of the C-P bond of the molecule $OPPh_3$. The evidence in the infrared spectrum of the photolyzed film of $Ni(PPh_3)_2Cl_2$ is therefore consistent with a product film of $Ni(OPPh_3)_2Cl_2$ (Equation 3.9).

$$Ni(PPh_3)_2Cl_2(s) + O_2(g) \xrightarrow{h\nu} Ni(OPPh_3)_2Cl_2(s) \qquad (3.9)$$

3.2.8. The chemistry of $Ni(PPh_3)_2Br_2$ films.

The ultraviolet spectrum of the $Ni(PPh_3)_2Br_2$ (1.44×10^{-5} M and 5.30×10^{-3} M in CH_2Cl_2) contained λ_{max}=262 nm, λ_{max}=434 nm and λ_{max}=574 nm corresponding to ε=29000 cm^{-1} M^{-1}, ε=5000 cm^{-1} M^{-1} and ε=200 cm^{-1} M^{-1} respectively. Giacometti et al[72] attribute the band at 262 nm as a ligand to metal charge transfer associated with the phosphine ligands. They attribute the band at 434 nm as ligand to metal charge transfer of the bromine ligand.

The infrared spectrum of the spin coated film of $Ni(PPh_3)_2Br_2$ was obtained and the most intense bands were identified. Bands at 692 cm^{-1} (strong), and 746 cm^{-1} (strong) correspond to vibrations in the phenyl rings.[66] The band at 1095 cm^{-1} (medium) corresponds to phosphorus carbon bending.[66]

The experimental procedure and results of the film of $Ni(PPh_3)_2Br_2$ are analogous to the procedures and results of the film of $Ni(PPh_3)_2Cl_2$. The film of $Ni(PPh_3)_2Br_2$ is thermally reactive with a half life of 138±20 hours. The infrared spectrum of the thermal and photo products contained bands at 542 cm^{-1}(strong), 692 cm^{-1} (strong), 746 cm^{-1} (medium), and 724 cm^{-1}(strong). Because the film sublimed under vacuum, the photochemistry experiments were done in air. Infrared spectra were obtained after 0, 20, 80, 160, 210, 400, 850 and 1100 minutes and the half life was 220 ±30 minutes. A sample of the spectra are given in Figure 3.6.

Figure 3.6: The photolysis of $Ni(PPh_3)_2Br_2$.

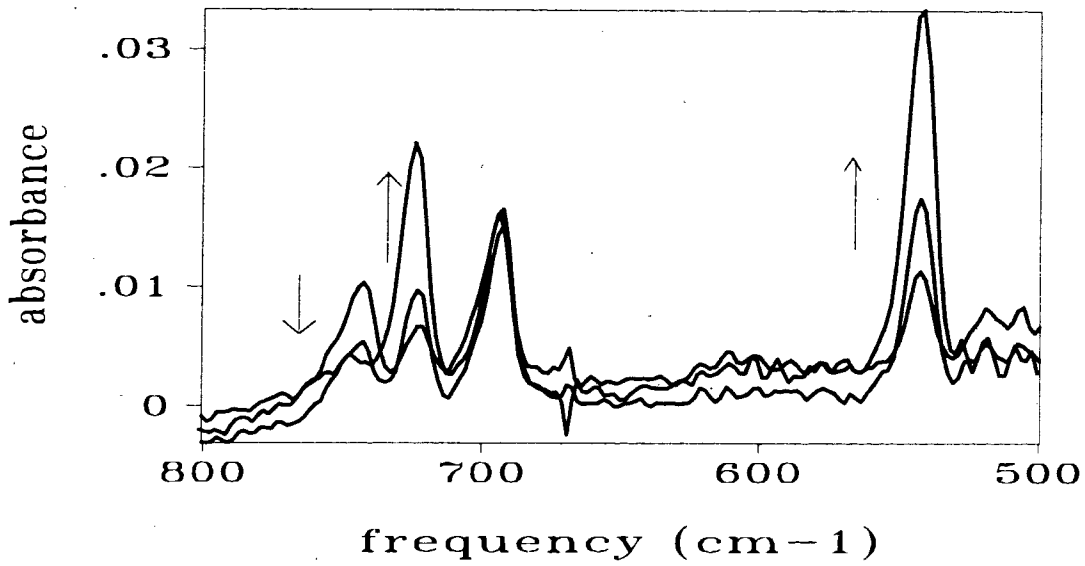

The infrared evidence of the photoproducts is consistent with the formation of $Ni(OPPh_3)_2Br_2$. The spectrum of the photoproduct contained bands at 542 cm^{-1}(strong), 692 cm^{-1} (strong), 746 cm^{-1} (medium), and 724 cm^{-1}(strong). By comparison, the bands of $OPPh_3$ are at 540 cm^{-1}(very strong), 690 cm^{-1} (strong), 720 cm^{-1} (strong) and 740 cm^{-1} (medium).[66] Based on the infrared evidence, the chemical reaction associated with $Ni(PPh_3)_2X_2$ is given in Equation 3.10.

$$Ni(PPh_3)_2Br_2(s) + O_2(g) \xrightarrow{h\nu} Ni(OPPh_3)_2Br_2(s) \qquad (3.10)$$

3.2.9. The chemistry of $Ni(PPh_3)_2I_2$ films.

The ultraviolet spectrum of the $Ni(PPh_3)_2I_2$ (1.58×10^{-5} M and 5.64×10^{-3} M in CH_2Cl_2) contained λ_{max}=262 nm, λ_{max}=438 nm and λ_{max}=574 nm corresponding to ε=8800 cm^{-1} M^{-1}, ε=11300 cm^{-1} M^{-1} and ε=500 cm^{-1} M^{-1} respectively. Giacometti et al[9] attribute the band at 262 nm as a ligand to metal charge transfer associated with the phosphine ligands. They attribute the band at 438 nm as ligand to metal charge transfer of the bromine ligand.

The infrared spectrum of the spin coated film of $Ni(PPh_3)_2I_2$ was obtained and the most intense bands were identified. Bands at 692 cm^{-1} (strong), and 743 cm^{-1} (strong) correspond to vibrations in the phenyl rings.[66] The band at 1095 cm^{-1} (medium) corresponds to phosphorus carbon bending.[66]

The film of $Ni(PPh_3)_2I_2$ was found to be thermally reactive with a half life of 19±3 hours. The infrared spectrum of the thermal product contained bands at 542 cm^{-1}(strong), 692 cm^{-1} (strong), 746 cm^{-1} (medium), and 724 cm^{-1}(strong).

Although the film did not sublime under vacuum, the photochemistry experiments were done in air to be consistent with the experiments done on $Ni(PPh_3)_2Cl_2$ and $Ni(PPh_3)_2Br_2$. Infrared spectra were obtained at 0, 11, 49, 98, 168, 368 minutes. The half life was 80±20 minutes.

The infrared evidence of the photoproducts is consistent with the formation of $Ni(OPPh_3)_2I_2$. The spectrum of the photoproduct contained bands at 542 cm^{-1}(strong), 692 cm^{-1} (strong), 746 cm^{-1} (medium), and 724 cm^{-1}(strong). By comparison, the bands of

$OPPh_3$ are at 540 cm^{-1}(very strong), 690 cm^{-1} (strong), 720 cm^{-1} (strong) and 740 cm^{-1} (medium).[66] Based on the infrared evidence, the chemical reaction associated with $Ni(PPh_3)_2I_2$ is given in Equation 3.11.

$$Ni(PPh_3)_2I_2(s) + O_2(g) \xrightarrow{h\nu} Ni(OPPh_3)_2I_2(s) \qquad (3.11)$$

3.4. Discussion

The photochemistry of a group of films of metal complexes containing halogen ligands was explored. The group of complexes that were spin coated for this purpose was $CpFe(CO)_2X_2$, $Ni(PEt_3)_2X_2$, and $Ni(PPh_3)_2X_2$ (X=Cl, Br, I). Amongst the complexes, it was found that metal oxides were successfully photodeposited from $CpFe(CO)_2I$. A variety of other photoproducts resulted from the photoreactivity of the remaining films, except $Ni(PEt_3)_2I_2$. Due to the thinness of the $Ni(PEt_3)_2I_2$ film, a photochemical reaction was not distinguishable. However, the photochemistries of the other films were pursued and the photoproducts were characterized. All had retained the halogen ligand(s) after photolysis. The photochemistry and photoproducts of each complex will be discussed. Because the precursor film of $CpFe(CO)_2I$ was a successful precursor to iron oxides, it will be discussed first and compared to the chlorine and bromine analogues. The discussion of the nickel complexes will follow.

The photoproduct of the film of $CpFe(CO)_2I$ was found to be an oxide of iron or a mixture of oxides of iron. The overall chemical reaction which is consistent with the

evidence of the study is given in Equations 3.5. In the proposed mechanism (3.6a-3.6c), the first step is photochemical loss of CO.

$$\tfrac{1}{2}\,O_2(g) + CpFe(CO)_2I \xrightarrow{h\nu} FeO + [Cp] + \tfrac{1}{2}\,I_2 + 2\,CO(g) \qquad (3.5)$$

$$CpFe(CO)_2I \xrightarrow{h\nu} CpFe(CO)I + CO(g) \qquad (3.6a)$$

$$CpFe(CO)I \rightarrow FeI + [Cp] + CO(g) \qquad (3.6b)$$

$$FeI + \tfrac{1}{2}O_2 \rightarrow FeO + \tfrac{1}{2}\text{ “I”} \qquad (3.6c)$$

The mechanism of the reaction of the film of $CpFe(CO)_2Cl$ (Equation 3.2a-3.2c) also includes the photochemical loss of CO. The overall reaction for $CpFe(CO)_2Cl$ is given in Equations 3.1. The reaction scheme for $CpFe(CO)_2Br$ is analogous.

$$\tfrac{1}{2}\,O_2 + CpFe(CO)_2Cl \xrightarrow{h\nu} FeOCl + [Cp] + 2\,CO(g) \qquad (3.1)$$

$$CpFe(CO)_2Cl \xrightarrow{h\nu} CpFe(CO)Cl + CO(g) \qquad (3.2a)$$

$$CpFe(CO)Cl \rightarrow FeCl + Cp + CO(g) \qquad (3.2b)$$

$$FeCl + \tfrac{1}{2}\,O_2 \rightarrow FeOCl \qquad (3.2c)$$

Loss of CO ligand in Equation 3.1 and 3.7 is a common photochemical reaction of $CpFe(CO)_2X$.[4, 17, 19] In solution for example, photosubstitution can occur with loss of a CO ligand and addition of a PPh_3 ligand.[4, 68] The electronic spectra reflect the tendency towards CO dissociation. The dominant absorption at 340, 350 and 336 nm for the chlorine, bromine and iodine analogues respectively are assigned to Fe→CO (π^*).[68] Pan et al[68] account for the absence of M-X homolysis by the lack of electronic bands assigned to either $X(\pi^*)\rightarrow M(\sigma^*)$ or $X(\sigma^*)\rightarrow M(\sigma^*)$.

Although CO loss is documented as the dominant photoprocess of $CpFe(CO)_2X$, there are examples of photoejection of the halogen ligand. Ali et al[69] monitored the photolysis of $CpFe(CO)_2Cl$ and $CpFe(CO)_2Br$ in DMSO and found that photoejection of halogen ligands resulted in shifts in energy of the CO stretches. The new bands were at 1984 cm^{-1} (strong), 1945 cm^{-1} (medium) and 1776 cm^{-1} (strong) in both analogues. In all of the spin coated films of $CpFe(CO)_2X$, new bands did not appear upon photolysis. This information is particularly relevant in determining the reaction scheme for the film of $CpFe(CO)_2I$. The absence of new bands throughout the photolysis of $CpFe(CO)_2I$, is consistent with the loss of the iodine during or after the photolytic loss of a carbonyl, but not before.

The AES and EDS results distinguished the photoproduct of $CpFe(CO)_2I$ as being a precursor to iron oxide. EDS results (section 3.2.3, Table 3.4) showed that the iodine atoms or ions had been ejected from the film. The amount of iodine remaining in the film was less than 1.5%. AES results (Table 3.5) indicated an iron to oxygen ratio of 1:1.4. The photoproduct film was amorphous and therefore it cannot be assigned to a known crystalline solid, however it can be loosely compared to crystalline solids. Based on the Auger results, the amorphous film approximately fits the ratio of the solids of Fe_2O_3 or Fe_3O_4 or a mixture of these two oxides.

The AES of the films of photolyzed $CpFe(CO)_2Cl$ and $CpFe(CO)_2Br$ showed a high content of chlorine and bromine respectively (Table 3.1-3.3). The ratio of Fe:O:X was approximately 1:1:1. FeOCl is a known compound,[10] and therefore one possibility may be the formation of FeOX for both the chlorine and bromine analogues.

As reaction reactions of 3.1 and 3.7 show, the photochemistries of the films $CpFe(CO)_2X$ are analogous to each other, but the subsequent thermal chemistries of 3.3 and 3.9 are different. Chlorine and bromine did not dissociate from the iron centre but the iodine did dissociate. This can be attributed to the bond energies of the Fe-X bond. In complexes of FeX_2, the bond energies are known to be 279, 340 and 400 kJ/mol for FeI_2, $FeBr_2$ and $FeCl_2$ respectively.[20] Therefore, in the three examples, there was a photochemical loss of CO, followed by a thermal loss of Cp and the other CO, and finally a thermal reaction which depended on the bond energy of the Fe-X bond.

The reaction of the photolyzed films of $Ni(PEt_3)_2Br_2$ that is consistent with the data is given in Equation 3.7. The reaction for the photolysis of the film of $Ni(PEt_3)_2Cl_2$ is analogous to the reaction of the $Ni(PEt_3)_2Br_2$.

$$Ni(PEt_3)_2Br_2 \xrightarrow{h\nu} NiBr_2 + [2\ PEt_3] \qquad (3.7)$$

The infrared evidence of the loss of $[PEt_3]$ was the decrease in intensity of the bands due to the corresponding P-C and C-H vibrations until they were no longer visible. A thermal reaction occurred simultaneously which was considerably slower but yielded the same infrared results. The photochemical reaction was distinguishable because of the shorter half lives of 240 and 100 minutes for the bromo and chloro analogues compared to the half lives of the thermal reaction which were 260 and 22 hours.

The possible loss of the bromine or chlorine ligand was determined by AES. It was found that neither halogen had been ejected from the film. The Auger spectra showed a varying amount of halogen in the film, as the film was sputtered. This was attributed to

preferential sputtering of the halogens. The AES results of the photolyzed films were compared to the AES results of a film of $NiBr_2$. The ratio of Ni:Br should theoretically be constant at 1:2, however the AES results showed a changing ratio with sputtering. Initially the ratio was 1:5, and after 20 seconds of sputtering, the ratio of Ni:Br was 1:2. Furthermore, the AES results of this film showed a substantial degree of carbon and oxygen contamination in the film (8.4% and 19.1% respectively) despite the 20 seconds of sputtering. Therefore, the carbon and oxygen detected in the photolyzed films of $Ni(PEt_3)_2X_2$ (X=Cl, Br) could also be wholly or partially a result of contamination.

The precursor films of $Ni(PPh_3)_2X_2$ (X=Cl, Br, and I) did not show loss of ligands upon photolysis or by thermal energy. The infrared spectra of $Ni(PPh_3)_2X_2$ films contained bands at 692 cm^{-1} and a band in the range 743-746 cm^{-1}, which both correspond to vibrations in the phenyl rings.[11] Both the photochemical and thermal reactions resulted in the generation of new bands at 542 cm^{-1}(strong), 724 cm^{-1}(strong) and 1090 cm^{-1} (m), in addition to the bands at 692 cm^{-1}(strong) and 747 cm^{-1}(medium). The generation of the new infrared bands is consistent with the formation of a -PPh_3O ligand. By comparison, the spectrum of free PPh_3O[10] contains a band at 540 cm^{-1}(very strong), 690 cm^{-1} (strong), 720 cm^{-1} (strong) and 740 cm^{-1} (medium), and 1095 cm^{-1}(medium). Therefore, the infrared data is consistent with the formation of $Ni(OPPh_3)_2X_2$ upon photolysis (Equation 3.12).

$$Ni(PPh_3)_2X_2(s) + O_2(g) \xrightarrow{h\nu} Ni(OPPh_3)_2X_2(s) \qquad (3.12)$$

3.4 Conclusion

The photolysis of films of spin coated $CpFe(CO)_2X$, $Ni(PEt_3)_2X_2$, and $Ni(PPh_3)_2X_2$ (X=Cl, Br, and I) were investigated. The main objective was to determine if the halogen ligands are ejected from the films upon photolysis. The ejection of ligands results in the photodeposition of a metal or metal oxide film (the metal film reacting with atmospheric oxygen).

We were successful in finding a complex which did eject all ligands. Upon photolysis, the film of $CpFe(CO)_2X$ produced a film of an oxide of iron. The ratio of Fe:O was approximately 1:1.4. In contrast, the Auger analysis of the photolyzed films of the chlorine and bromine analogues showed that the ratio of Fe:O:Cl or Fe:O:Br was 1:1:1. Possible products are the films of FeOCl and FeOBr. The weaker Fe-I bond compared to the bonds of Fe-Cl and Fe-Br is attributed to the difference in reactivity of the three films of $CpFe(CO)_2X$.

None of the films of the $Ni(PEt_3)_2X_2$, and $Ni(PPh_3)_2X_2$ reacted to make films of nickel or nickel oxide. The approximate ratio of 1:2 of Ni:Cl and Ni:Br is consistent with films of $NiCl_2$ and $NiBr_2$. It was not clear that the film of $Ni(PEt_3)_2I_2$ reacted photochemically and therefore, this film was not discussed further. The three films of $Ni(PPh_3)_2X_2$ did not show loss of ligands in the infrared spectra. The spectra of the photoproducts were consistent with films of $Ni(OPPh_3)_2X_2$.

Results of this chapter do show that it is possible to make films of metal and metal oxides by photolyzing spin coated films of halogen containing metal complexes. Further

studies could identify precursor films that could be used industrially in the photodeposition of metal and metal oxide films.

3.5. Experimental Section.

Silicon wafers were P-type Si(111) and were obtained from Pacific Microelectronics Centre. They were cut into approximately 1x1 cm^2 for the spin coating process. All the chips were cleaned in reagent grade CH_2Cl_2 before spin coating. The spin coating was done with a Laurell Technology Co. spin coater. All of the films were viewed under a Leitz light microscope to assess their quality in terms of crystallinity. Fourier transform infrared (FTIR) spectra were recorded with a Bomen MB-120 spectrophotometer on samples held in an aluminum chamber by steel clips. Ultraviolet-visible spectra measurements were obtained with an HP 8452 diode array spectrophotometer. Auger spectra were obtained by Dr. Sharon L. Blair. Auger spectra were obtained using a PHI double pass CMA at 0.85 eV resolution with 3kV ionization electron beams. Sample sputtering was done using 3 kV electron beam of Argon. The energy dispersive spectra were done by Dr. Albert Curzon's research laboratory in the Department of Physics at Simon Fraser University.

3.5.1. The syntheses of Cyclpentadienyliron Dicarbonyl Halides $CpFe(CO)_2X$ (X=Cl, Br, I).

a) The Synthesis of Cyclopentadienyliron Dicarbonyl Chloride - $CpFe(CO)_2Cl$.

This complex was prepared by the literature method of Piper, Cotton and Wilkinson.[61]

To a solution of $(CpFe)_2Fe(CO)_4$ (0.7032 g) in EtOH (25 mL), and $CHCl_3$ (10 mL), concentrated HCl (36-38%) was added (1.5 mL). Air was bubbled into the mixture until the red color of the solution became clear (2 h). The solvent was evaporated under vacuum, and the residue was dissolved in distilled water (10 mL). The solution was filtered and the title compound was extracted from the aqueous media with $CHCl_3$ (3x10 mL). The organic extract was concentrated and petroleum ether was added. The title compound crystallized. After cooling, the product was filtered, washed with cold petroleum ether and dried under vacuum overnight.

Analysis for $C_7H_5O_2FeCl$. Calcd.: C, 39.58; H, 2.37. Found: C, 40.11; H, 2.55.

b) The Synthesis of Cyclopentadienyliron Dicarbonyl Bromide $CpFe(CO)_2Br$.

This complex was prepared by the literature method of Hallan and Pauson.[62]

To a solution of $(CpFe)_2Fe(CO)_4$ (0.7032 g) in EtOH (25 mL), and $CHCl_3$ (12.5 mL), hydrobromic acid 48% was added (2.5 mL). Air was bubbled into this brown solution for 3.5h. The solvent was evaporated under vacuum and the residue dissolved in $CHCl_3$ (30 mL). The solution was filtered through a pad of neutral alumina and the solvent was concentrated. Petroleum ether was added. The title compound crystallized. The crystals were filtered, washed with cold petroleum ether and dried under vacuum overnight.

Analysis for $C_7H_5O_2FeBr$. Calcd.: C, 32.73; H, 1.96. Found: C, 30.51; H, 2.01.

c) The Synthesis of Cyclopentaldienyliron Dicarbonyl Iodide $CpFe(CO)_2I$.

This complex was prepared by the literature method of Piper and Wilkinson.[63]

Iodine (0.5 g) was added to a solution of $CpFe_2(CO)_4$ (0.500 g) in $CHCl_3$ (75 mL). The mixture was stirred at room temperature. After all the iodine was dissolved (0.5 h) the chloroformic solution was shaken with an aqueous solution of sodium thiosulphate to remove any unreacted iodine. After separation of the two layers, the organic solution was evaporated away under vacuum to afford a brown solid. This solid was dissolved in a minimum amount of chloroform and then petroleum ether was added. The title compound crystallized. The product was filtered, washed with cold petroleum ether, and dried under vacuum.

Analysis for $C_7H_5O_2FeI$. Calcd.: C, 27.67; H, 1.66. Found: C, 27.72; H, 1.61.

d) The syntheses of $Ni(PPh_3)_2X_2$ and $Ni(PEt_3)_2X_2$ (X=Cl, Br, I) are described in section 2.5.1.

3.5.2. Experimental procedure for $CpFe(CO)_2Cl$.

The $CpFe(CO)_2Cl$ was dissolved in CH_2Cl_2 (1.4×10^{-5} M). The ultraviolet-visisble spectra of the solution was taken in a 1 cm x 1 cm cuvette.

A film of $CpFe(CO)_2Cl$ was prepared by the method described in section 1.2. The film was mounted in the infrared chamber as illustrated in Figure 3.7.

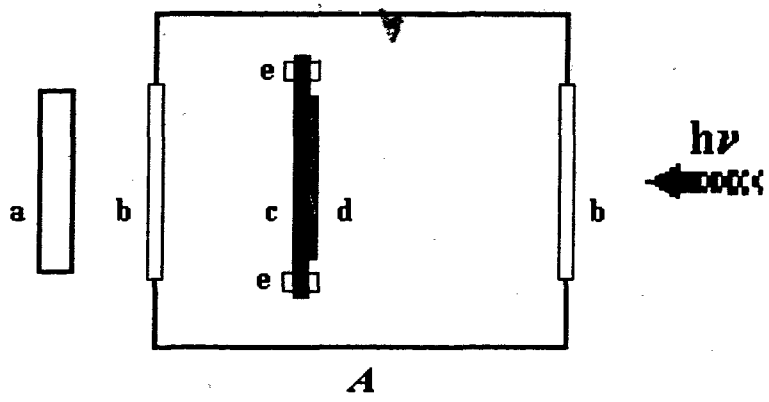

Figure 3.7. Diagram of the photo-reaction instrumentation and FTIR recording. ***A***. Photo-chamber. **a**. Infrared detector. **b**. Sodium chloride window. **c**. Silicon chip. **d**. Thin film. **e**. Steel clips to hold the silicon chip (**c**). **hν**. Electromagnetic beam (IR).

An infrared spectrum was obtained of the $CpFe(CO)_2Cl$ film. Another spectrum was taken after the sample remained in the dark and at room temperature for 24 hours. The spectrum did not change during the 24 hour period, indicating a thermally stable film. A film of $CpFe(CO)_2Cl$ was also monitored under vacuum, in the dark, and at room temperature. After 10 minutes, the film had sublimed in the chamber.

Another spin coated film of $CpFe(CO)_2Cl$ was mounted in the infrared chamber and put under a nitrogen atmosphere. The infrared spectrum was obtained, followed by a timed exposure to water filtered light energy from a mercury lamp. Another spectrum was obtained and the experiment proceeded with alternating timed exposures to light interrupted by spectral analysis. Spectra were taken after 0, 10, 30, 55, 85, 120, and 270 minutes of photolysis.

The film photolyzed from $CpFe(CO)_2Cl$ was submitted for AES analysis.

3.5.3. Experimental procedure for $CpFe(CO)_2Br$.

The $CpFe(CO)_2Br$ was dissolved in CH_3CN (1.5×10^{-5} M). The ultraviolet-visisble spectra of the solution was taken in a 1 cm x 1 cm cuvette.

The procedure for the films of $CpFe(CO)_2Cl$ was followed for the films of $CpFe(CO)_2Br$ film. The only difference was that the spin coating solution for $CpFe(CO)_2Br$ was in CH_3CN and that the timed intervals of photolysis were 9, 17, 28, 36, 47, and 62 minutes of photolysis.

The film of photolyzed $CpFe(CO)_2Br$ was submitted for AES analysis.

3.5.4. Experimental procedure for $CpFe(CO)_2I$.

The $CpFe(CO)_2I$ was dissolved in CH_2Cl_2 (1.5×10^{-5} M). The ultraviolet-visisble spectra of the solution was taken in a 1 cm x 1 cm cuvette.

The procedure for the films of $CpFe(CO)_2Cl$ was followed for the films of $CpFe(CO)_2I$ film. The timed intervals of photolysis were 0, 15, 40, 75, 90, and 720 minutes of photolysis.

The film of photolyzed $CpFe(CO)_2Br$ was submitted for AES analysis and EDS analysis.

3.5.5. Experimental procedure for $Ni(PEt_3)_2Cl_2$.

The $Ni(PEt_3)_2Cl_2$ was dissolved in CH_2Cl_2 (2.06×10^{-5} M and 6.67×10^{-3} M). The ultraviolet spectrum of the solution was taken in a 1 cm x 1 cm cuvette.

A film of $Ni(PEt_3)_2Cl_2$ was prepared by the method described in section 2.5.2. The film was mounted in the infrared chamber as illustrated in Figure 3.1.

An infrared spectrum was obtained of the $Ni(PEt_3)_2Cl_2$ film. Spectra were taken after the sample had been in the dark and at room temperature for 24 hours and two weeks. The bands of the spectra decreased in intensity with a half life of 22±4 hours, indicating thermal reactivity. A film of $Ni(PEt_3)_2Cl_2$ was also monitored under vacuum, in the dark and at room temperature. After 10 minutes the film had sublimed.

A spin coated film of $Ni(PEt_3)_2Cl_2$ was mounted in the infrared chamber in air. The infrared spectrum was obtained, followed by a timed exposure to water filtered light energy from a mercury lamp. Another spectrum was obtained and the experiment proceeded with alternating timed exposures to light interrupted by spectral analysis. Spectra were taken after 0, 30, 120, 300, and 1200 minutes of photolysis. The experiment was stopped when the bands had decreased in intensity until they were no longer visisble. The half life was 100±20 minutes.

The film photolyzed from $Ni(PEt_3)_2Cl_2$ was analyzed by AES.

3.5.6. Experimental procedure for $Ni(PEt_3)_2Br_2$

The procedures followed for the experiments with the complex $Ni(PEt_3)_2Br_2$ were the same as the procedures followed for the experiments with $Ni(PEt_3)_2Cl_2$. The ultraviolet spectrum was obtained from of solutions of 1.93×10^{-5} M and 4.85×10^{-3} M. The half life of the thermal reaction was 260±30 hours. The photochemical reaction had a half life of 240±30 minutes. Spectra were taken after 0, 20, 90, 150, 210, 310, and 1750 minutes of photolysis. It was observed that the photoproduct was deliquescent. The photoproduct was analyzed by AES. A sample of $NiBr_2$ was also analyzed by AES to compare with the photoproduct of $Ni(PEt_3)_2Br_2$.

3.5.7. Experimental procedure for $Ni(PEt_3)_2I_2$.

The ultraviolet spectrum of the $Ni(PEt_3)_2I_2$ in CH_2Cl_2 (2.16×10^{-5} M and 6.49×10^{-3} M) was obtained. The infrared spectra however were difficult to interpret however because the intensity of the bands were low in comparison to the noise. Further experiments were not done on the films of $Ni(PEt_3)_2I_2$.

3.5.8. Experimental procedure for $Ni(PPh_3)_2Cl_2$.

The ultraviolet spectrum of the complex of $Ni(PPh_3)_2Cl_2$ in CH_2Cl_2 (1.54×10^{-5} M and 6.02×10^{-3} M) was obtained. The procedure of experiments of the spin coated films

of $Ni(PPh_3)_2Cl_2$ were the same as they were for the films of $Ni(PEt_3)_2Cl_2$ except that the photoproducts of $Ni(PPh_3)_2Cl_2$ were not analyzed by AES. During photolysis spectra were obtained at 0, 7, 32, 72, 130, 190, and 1070 minutes. The final spectrum contained new bands which were not present in the initial spectrum.

3.5.9. Experimental procedure for $Ni(PPh_3)_2Br_2$.

The ultraviolet spectrum of the complex of $Ni(PPh_3)_2Br_2$ in CH_2Cl_2 (1.44×10^{-5} M and 5.30×10^{-3} M).

The procedure of experiments of the spin coated films of $Ni(PPh_3)_2Br_2$ were the same as they were for the films of $Ni(PEt_3)_2Cl_2$ except that the photoproducts of $Ni(PPh_3)_2Br_2$ were not analyzed by AES. Infrared spectra were taken at 0, 20, 80, 160, 210, 400, 850, and 1100 minutes of photolysis.

3.5.10. Experimental procedure for $Ni(PPh_3)_2I_2$.

The ultraviolet spectrum of the complex of $Ni(PPh_3)_2I_2$ in CH_2Cl_2 (1.58×10^{-5} M and 5.64×10^{-3} M).

The procedure of experiments of the spin coated films of $Ni(PPh_3)_2I_2$ were the same as they were for the films of $Ni(PEt_3)_2Cl_2$ except that the photoproducts of $Ni(PPh_3)_2I_2$ were not analyzed by AES. During photolysis spectra were obtained at 0, 11, 49, 98, 168, and 368 minutes.

References

1. M. Ohring, The Materials Science of Thin Films, Academic Press, Inc., Toronto, (1992)

2. D. L. Smith, Thin Film Deposition: Principles & Practice, McGraw-Hill, Inc., Toronto, (1995)

3. D.V. Morgan, K. Board, and R.H. Cockrum, An Introduction To Micorelectronic Technology, John Wiley & Sons, Toronto, (1985)

4. J. M. E. Harper, Thin Film Processes, Academic Press, New York, (1978)

5. Thin Film Processes II, Edited by J. L. Vossen, and W. Kern, Academic Press, Inc., San Diego, (1991)

6. D. E. Bornside, C. W. Macosko, and L. E. Scriven, *J. Imag. Tech.*, **13**, 123 (1987)

7. Meihua Gao, Solid state Photochemistry of Uranyl Carboxylate and 1,3-Diketonate Complexes: Photochemical Patterning of Uranium Oxide Lines via Uranyl Complex Thin Film Precursors, M. Sc. Thesis, Simon Fraser University, Burnaby, B.C., (1995)

8. R. H. Hill, S. L. Blair, C. W. Chu, M. Gao, C. I. Horvath, and B. J. Palmer, *Trends in Photochemistry and Photobiology,* **3**, 331-338 (1994)

9. R. H. Hill, A. A. Avey, S. L. Blair, M. Gao, and B. J. Palmer, *Materials Chemistry and Physics,* **43**, 233-237 (1996)

10. W. S. Ruska, Microelectronic Processing An Introduction to the Manufacture of Integrated Circuits, McGraw-Hill Book Company, Toronto, (1987)

11. Unpublished results: Optically amorphous films of $Co(PEt_3)_2(NO_3)_2$ showed spectroscopic evidence of photoreactivity, while crystallized films of $Co(PEt_3)_2(NO_3)_2$ did not.

12. L.M. Venanzi, *J. Chem. Soc.*, 719-724 (1958)

13. K.A. Jensen, *Z. Anorg. Allg. Chem.*, **229**, 225-263 (1936)

14. F.A. Cotton, O.D. Faut, and D.M.L. Goodgame, *J. Am. Chem. Soc.*, **83**, 344-351 (1961)

15. C. A. McAuliffe, Transition Metal Complexes Containing Phosphine Ligands, John Wiley and Sons, Toronto, (1973)

16. G. Garton, D.E. Henn, H. M. Powell, and L.M. Venanzi, *J. Chem. Soc.*, 3625-3629 (1963)

17. P.L. Goggin, and R.J. Goodfellow, *J. Chem. Soc. (A)*, 1462-1466 (1966)

18. V. Scatturin, and A. Turco, *J. Inorg. Nucl. Chem.*, **8**, 447-451 (1958)

19. P.M. Boorman, and A. J. Carty, *Inorg. Nucl. Chem. Lett.*, **4**, 101-105 (1968)

20. K. Shobatake, and K. Nakamoto, *J. Am. Chem. Soc.*, **92**, 3332-3335 (1970)

21. J. H. S. Green, *Spectrochem. Acta*, **24A**, 137-143 (1968)

22. N. H. Turner, The Handbook of Surface Imaging and Visualization, "Auger Electron Spectroscopy", Edited by A. T. Hubbard, CRC Press, Boca Raton, Florida, (1995)

23. G. C. Smith, Surface Analysis by Electron Spectroscopy: Measurement and Interpretation, Plenum Press, New York, (1994)

24. S. L. Blair, W. Xia, and R. H. Hill, *J. Photochem. Photobiol. A.* **81**, 183-191 (1994)

25. P. M. Boorman, and A. J. Carty, *Inorg. Nucl. Chem. Lett.*, **4**, 101-105 (1968)

26. K. Shobatake, and K. Nakamoto, *J. Am. Chem. Soc.*, **92**, 3332-3335 (1970)

27. J. H. S. Green, *Spectrochem. Acta*, **24A**, 137-143 (1968)

28. W. K. Daughton, and F. L. Givens, *J. Electrochem. Soc.:Solid State Science and Technology*, **129**, 173-179 (1982)

29. J. E. Fergusson, and P. F. Heveldt, *Inorg. Chim. Acta*, **31**, 145-154 (1978)

30. G. Booth, Advances in Inorganic Chemistry and Radiochemistry, "Phosphine Arsine and Stibine Complexes", **6**, 27-32 (1964)

31. J. A. J. Jarvis, R. H. B. Mais, and P. G. Owston, *J. Chem. Soc. (A) Inorg. Phys. Theor.*, 1473-1486 (1968)

32. CRC Handbook of Chemistry and Physics *Seventieth Edition*, Edited by R. C. Weast, D. R. Lide, M. J. Astle, and W. H. Beyer, CRC Press Inc., Boca Raton, Florida, (1990)

33. G. F. Damon, "Proceedings of the Second Kodak Seminar on Microminiaturization," Eastman Koday Co., Rochester, New York, (1967)

34. D. Meyerhofer, *J. Appl. Phys.*, **49**, 3993-3997 (1978)

35. J. H. Lai, *Polym. Eng. Sci.*, **19**, 1117-1121 (1979)

36. B.T. Chen, *Polym. Eng. Sci.*, **23**, 399-403 (1983)

37. G. E. Anner, Planar Processing Primer, Van Nostrand Reinhold, Scarborough, (1990)

38. N. Talahashi, N. Kakuda, S. Ueno, and K. Uamaguchi, Fuji, *Jpn. J. Appl. Phys.*, **28**, L244-L247 (1989)

39. T. Patton, Paint flow and Pigment Dispersion *Second Edition*, chapter 30, Wiley Interscience Publication, John Wiley & Sons, Toronto, (1979)

40. S. A. Jenekhe, and S. B. Shuldt, *Ind. Eng. Chem.*, **23**, 432-436 (1984)

41. S. A. Jenekhe, *Polym. Eng. Sci.*, **23**, 830-834 (1983)

42. R. Eaton, and F. Willeboordse, *J. Coating Tech.*, **52**, 63-70 (1980)

43. P. Sukanek, *J. Imag. Tech.*, **11**, 184-190, (1985)

44. A. G. Emslie, F. T. Bonner, and L. G. Peck, *J. Appl. Phys.*, **29**, 858-862 (1958)

45. W. W. Flack, D. S. Soong, A. T. Bell, and D. W. Hess, *J. Appl. Phys.*, **56**, 119-1206 (1984)

46. B.D. Washo, *IBM J. Res. Development*, **21**, 190-198 (1977)

47. W. A. Levinson, A. Arnold, and O. Dehodgins, *Polym. Eng. Sci.*, **33**, 980-988 (1993)

48. K. J. Skrobis, D. D. Denton, and A. V. Skrobis, *Polym. Eng. Sci.*, **30**, 193-196 (1990)

49. P. Sukanek, *J. Electrochem. Soc.*, **138**, 1712-1719 (1991)

50. T. Yada, T. Maejima, M. Aoki, and M. Umesaki, *Jpn. J. Appl. Phys.*, **34**, 6279-6284 (1995)

52. F. Wang, A. Uusimaki, S. Leppavuori, and H. Zhang, *Mater. Res. Bull.*, **31,** 37-46 (1996)

53. P. Li, and L. F. Francis, *J. Mater. Sci.*, **30**, 6192-6204 (1995)

54. Langes Handbook of Chemistry *Twelfth Edition*, Edited by J. A. Dean, formally Compiled and Edited by N. A. Lange, Toronto, (1979)

55. C.W. Frank, V. Rao, M. M. Despotopoulou, R. F. W. Pease, W.D. Hinsberg, R.D. Miller, and J. F. Rabolt, *Science,* **273**, 912-915 (1996)

56. R. G. J. Miller, *XII Colloquium Spectroscopium Internationale,* 523-539, Helger & Watts, Exeter, (1965)

57. F. A. Cotton, A. D. Liehr, and G. Wilkinson, *J. Inorg. Nucl. Chem.*, **1,** 175-186 (1955)

58. H. B. Abrahamson, M. C. Palazzotto, C. L. Reichel, and M. S. Wrighton, *J. Am. Chem. Soc.*, **101**, 4123-4127 (1979)

59. A. F. Hepp, J. P. Blaha, C. Lewis, and M. S. Wrighton, *Organometallics*, **3**, 174-177 (1984)

60. D. F. Alway, and K. W. Barnett, *Inorg. Chem.*, **10**, 2826-2831 (1978)

61. T. S. Piper, F. A. Cotton, and G. Wilkinson, *J. Inorg. Nucl. Chem.*, **1**, 165-174 (1955)

62. B. F. Hallam, and P. L. Pauson, *J. Chem. Soc.*, 3030-3037 (1956)

63. T. S. Piper, and G. Wilkinson, *J. Inorganic and Nuclear Chemistry,* **2**, 38-45 (1956)

64. C.R.C. Courssmaker, M. Hely Hutchinson, J.R. Mellor, L.E. Sutton, and L.M. Venanzi, *J. Chem. Soc.*, 2705-2713 (1961)

65. F. A. Cotton, and G. Wilkinson, Advanced Inorganic Chemistry *Fifth Edition*, John Wiley & Sons, Toronto, (1988)

66. K. A. Jensen, and P. H. Nielsen, *Acta Chem. Scand.*, **17**, 1875-1885 (1963)

67. D. G. Bickley, R. H. Hill, and C. I. Horvath, *J. Photochem. Photobiol. A: Chem.*, **67** 181-186 (1992)

68. X. Pan, C. E. Philbin, M. P. Castellani, and D. R. Tyler, *Inorg. Chem.* **27**, 671-676 (1988)

69. L. H. Ali, A. Cox, and T. J. Kemp, *J. Chem. Soc. Dalton Trans.*, 1475-1478 (1973)

70. R. H. Hooker, K. A. Mahmoud, and A. J. Rest, *J. Chem. Soc. Dalton Trans.*, 1231-1241 (1990)

71. J. E. Huheey, Inorganic Chemistry; Principles of Structure and Reactivity *Third Edition*, Appendix 3, Harper and Row, New York, (1983)

72. G. Giocometti, and A. Turco. *J. Inorg Nucl. Chem.*, **15**, 242-249 (1960)

73. The New Lexicon Webster's Encyclopedic Dictionary of the English Language Canadian Edition, Lexicon Publications, Inc., New York, (1988)

74. H. Blatt and R. J. Tracey, Petrology: Igneous, Sedimentary, and Metamorphic *Second Edition*, page 39, W. H. Greeman & Company, New York, (1996)